Kelley, Douglas I.; Bistinas, Ioannis; Whitley, Rhys; Burton, Chantelle; Marthews, Toby R.; Dong, Ning. 2019. **How contemporary bioclimatic and human controls change global fire regimes**. *Nature Climate Change*, 9 (9). 690-696. https://doi.org/10.1038/s41558-019-0540-7

How contemporary bioclimatic and human controls change global fire regimes.

Douglas I. Kelley[1,*], Ioannis Bistinas[2,3], Rhys Whitley[4], Chantelle Burton[5], Toby R. Marthews[1], Ning Dong[6,7]

1: Centre for Ecology and Hydrology, Wallingford OX10 8BB, U.K.

2: ATOS Nederland B.V., Burgemeester Rijnderslaan 30, 1185 MC Amstelveen, The Netherlands

3: Vrije Universiteit Amsterdam, Faculty of Sciences, Department of Earth Sciences, De Boelelaan 1085, 1081 HV, Amsterdam, The Netherlands

4: Natural Perils Pricing, Commercial and Consumer Portfolio and Product, Suncorp Group, Sydney, Australia

5: Met Office Hadley Centre for Climate Science and Services, Exeter, UK

6: School of Archaeology, Geography and Environmental Sciences (SAGES), University of Reading, Whiteknights, Reading RG6 6AB, United Kingdom

7: Department of Biological Sciences, Macquarie University, North Ryde, NSW 2109, Australia

* *Corresponding Author*

Summary

Fires play an important role in ecosystem dynamics. Long-term controls on global burned area include fuel continuity and moisture, with ignitions and human activity becoming dominant in specific ecosystems. Changes in fuel continuity and moisture are the main drivers of changes of fire globally.

Introductory paragraph

Anthropogenically driven declines in tropical savanna burnt area [1,2], have recently received much attention due to their impact on trends in global burnt area [3,4]. Large-scale trends in ecosystems where vegetation has adapted to infrequent fire, especially in cooler and wetter forested areas, are less well understood. Here, small changes in fire regimes can have a substantial impact on local biogeochemistry [5]. In order to investigate trends in fire across a wide range of ecosystems, we used Bayesian inference [6] to quantify four primary controls on burnt area: fuel continuity; fuel moisture; ignitions; and anthropogenic suppression. We found that fuel continuity and moisture are the dominant limiting factors of burnt area globally. Suppression is most important in cropland areas, whereas savannas and boreal forests are most sensitive to ignitions. We quantify fire regime shifts in areas with multiple, and often counteracting trends in these controls. Forests are of particular concern, where we show average shifts in controls of 2.3-2.6% of their potential maximum per year, primarily driven by trends in fuel continuity and moisture. This study gives added importance to understanding long-term, future changes in the controls on fire and the impact of fire trends on ecosystem function.

Main text

Fire-prone tropical ecosystems account for 78% of global burnt area, despite covering just 16% of the land surface [7]. Consequently, changes in these fire regimes have a disproportionate impact on trends in global burnt area. Contribution from less-fire prone ecosystems to the global signal is less certain, and given the significance of multiple bioclimatic controls in limiting fire, it is difficult to distinguish any prime, dominant driver [2,8,9]. To determine what drivers are in these areas requires an assessment of the interplay of different controls on burnt area, which may also highlight potential shifts in fire regimes not detectable via trend analysis of burnt area alone.

Fire danger indices can be used to quantify the influence of trends in climate on fire weather [10,11], providing policy-relevant information for fire management [12]. However, they often exclude the effects of fuel dynamics, ignitions and human activity, and it can be hard to relate indices to observable fire variables useful in global analyses [13]. Fire-enabled terrestrial biosphere models (TBMs) can account for these drivers [5,13,14]. However, most TBMs fail to reproduce trends in fire reliably, and even disagree on basic spatial patterns and magnitudes of burnt area [1,2] due to missing descriptions of key anthropogenic processes suppressing fire and an imbalance in the relative strength of bioclimatic controls [2,8,15]. Conversely, studies aimed at determining the strength of human and bioclimatic influences on burnt area from observations often correlate individual drivers with burnt area in isolation [2,16] and so do not consider the complex interaction of multiple drivers. This has led to calls for frameworks that fuse statistical representations of fire drivers with modelling techniques that consider such interactions [17,18]. One such technique is the “Resource Gradient Constraint” framework [16,19–21], which applies changes in climate drivers to a static representation of vegetation [19,20]. However, this approach relies on either invariant or modelled fuel controls, often through the interpretation of changes in moisture drivers. With this in mind, Bistinas et al [15] used generalised linear modelling to quantify the relative strength of human and bioclimatic drivers in the presence of all other drivers, thereby allowing climate, biotic, ignition and human drivers a more causal influence on burnt area. Using a similar technique, [7] mapped the relative limitations imposed by fuel load, fuel moisture and ignitions controls for Australia by selecting one key driver from [15] for each control. This was subsequently developed to incorporate multiple drivers into each of these three controls [20] and expanded globally with the inclusion of a fourth control: human suppression [8].

Here, we assess trends in four controls of burnt area in order to identify changes in global fire regimes. Controls combine burnt area drivers identified in [8,15,16,20] or which are used widely by the global fire modelling community [19,22]. The four controls consisted of: (1) fuel continuity (referred to as "fuel"), which increases burnt area, is driven by vegetation cover and a fine fuel accumulation proxy [16,19,20] (Supplementary Fig. 1); (2) moisture, which decreases burning, combines proxies for live and dead fuel; (3) natural and anthropogenic potential ignitions ("ignitions") which increase burning; and (4) anthropogenic suppression, decreasing burning, is driven by population fire suppression and land-use fragmentation. Supplementary Table 1 and Supplementary Fig. 2,3 contain information on drivers and data sources. Burnt area in our model is reduced according to the strength of each of these controls (Fig. 1, see methods), an approach followed by most global fire models [22]. Controls, along with the contribution of each driver to their controls, were optimised against 2000-2014 monthly burnt area observations from GFED4s [23] using iterative Bayesian inference [6] allowing us to quantify the uncertainty of the resultant parameters and control contribution.

Our reconstructed burnt area reproduces the magnitude and spatial extent of annual burning and associated trends, with relatively little spread accounting for parameter uncertainty (Supplementary Table 2 and Supplementary Fig. 6). We reproduce the maximum burning at intermediate fuels and moisture due to covariance in optimised fuel and moisture controls [14,19,24], with a reduction in burnt area at fuel continuities greater than 60% and moisture of less than 5% (Supplementary Fig. 7). Low population densities only increase burning at specific times of the year, and in just a few areas (8.76±6.96% of land coverage) and always decrease burning in areas with low or no suppression from cropland (Supplementary Fig. 8). Population densities above 288±145 people/km^2 reduce burnt area by 50%. The impact of suppression also increases rapidly at low cropland cover, limiting burnt area to 50% at 10.36±0.12% cover.

Globally, fuel has the largest mean (or “standard”) limitation (points along the curves in Fig. 1), followed closely by ignitions when considered in isolation from other controls (Supplementary Fig. 9), as is standard in many control studies [7,8]. However, burnt area only increases by 3.48±0.05% if ignition limitation is removed due to the presence of the other controls - much smaller than the increase in burnt area from removing limitation from fuel (21.36±0.84%), moisture (9.82±0.07%) and suppression (4.51±0.01%) (Supplementary Table 3). We define this measure of determining control strength as the “potential limitation” (Fig. 2a). In arid ecosystems, ignitions show a substantial and significant standard limitation due to little human impact or lightning (Supplementary Table 3). However, as there isn’t any fuel, the introduction of ignitions has no impact on burnt area. Conversely, increasing vegetation cover would lead to a small but significant increase in fire, given the lack of burning. The difference between standard and potential limitation is even more important in boreal regions, where the standard misses the distinction between moisture-limited Northern Europe, western Siberia and southern Canada, and ignition-limited eastern Siberia, Alaska and the Canadian tundra. Rainforests show highly variable and occasionally substantial standard fuel limitation (Fig. 2, Supplementary Table 3) due to variations in herbaceous cover (Supplementary Fig. 2); a possible consequence of differences in canopy gap frequency effects on understorey vegetation from variations in topography, soils and disturbance [25,26]. This variation in forest fuel becomes less important when considering potential limitations due to the strength of moisture controls.

More relevant for potential short-term changes in burnt area is its "sensitivity", or rate of change, given a small change in a control. We attributed changes in burnt area over our study period to trends in these sensitivities by calculating the annual average difference between burnt area reconstructed with and without the trends in each control (see methods). While we were able to test the sensitivity of burnt area to ignitions as a whole, changes in lightning ignitions were not incorporated into our assessment of trends in controls because of data availability. During the fire season, burnt area in most tropical savannas is unconstrained except occasionally by human suppression (Supplementary Fig. 9). However, these ecosystems show the highest sensitivity to human suppression (Supplementary Fig. 9f; Supplementary Table 3) which, due to increases in cropland and population density [2], are attributed as the main cause for their recent, rapid decline in burnt area (Fig. 3c, 4). This is slightly offset by population-driven increases in ignitions which savannas are also sensitive to. Our results also indicate increases in suppression in tropical wet forests, particularly in Indonesia (Fig. 3, Supplementary Fig. 10) and in the southern end of the Amazon arc of deforestation, where changes in fire have already been attributed to a shift in agricultural practices from pasture to cropland [27] (Supplementary Fig. 3). Conversely, suppression decreases in areas of land-use recession and reforestation in mediterranean and temperate areas throughout North America and Europe [28].

Fuel and moisture trends are more important than direct human influence in most parts of the world (Fig. 5). Increases in vegetation cover decrease fuel limitation in arid and semi-arid ecosystems, affecting 75±2% of all mediterranean and desert ecosystems and 63±6% of tropical savanna (Fig. 4). Drying conditions are causing a shift in the Kazakhstan/Russia fire zone, with Ural/Siberian boreal forests to the north becoming drier and more susceptible to fire, and more sparse vegetation cover reducing fire in Kazakhstan (Fig. 3c). Boreal and temperate forests in North America and Central Europe show a change in moisture control, of a similar magnitude that leads to lower fire incidence. In some areas of the Siberian boreal region, increases in fuel from increased vegetation cover coincide with decreases in moisture - both possibly driven by increases in temperature due to the accelerated warming at high latitudes [29] (Supplementary Fig 2). Likewise, increased vegetation cover in dry grassland and shrubland areas of Central Australia, South Africa and South America show increased fuel, sometimes alongside decreasing moisture. Reduced moisture limitation in China's tropical and warm temperate forests are compounded by a retreat in cropland cover, reducing suppression and increasing fuel (Fig. 3d-f, Supplementary Fig. 3,10). Conversely, some areas of deforestation in the tropical western and northern Amazon and the Congo coincide with areas of increased moisture, both driving a decrease in burnt area.

In most other non-arid ecosystems fuel trends correlate with moisture. As fuel and moisture have opposing effects on burnt area, their trends dampen each other's impact on changes in burnt area (Supplementary Fig. 7). There is, therefore, a potential for a shift in controls on fire of a greater magnitude than identified through changes in burnt area alone. We used both the absolute change in burnt area over mean burnt area (Fig. 3a) and how much each control deviated from its trendless "potential" as a percentage of maximum deviation (Fig. 3b) as indices of fire regime shift. This quantifies the total change in burnt area that would be masked by the actual mean (Fig. 4). Globally, fire controls showed a shift of 26.88±0.35% during our study period; almost twice as high as the 14.23±0.48% trend in burnt area (Fig. 4,5). Despite the focus on the contribution of tropical savanna to the trend in the global burnt area [2], forests are much more susceptible to a shift in regime, with an average shift in absolute burnt area of 0.88-0.96% in savanna compared to 1.10-1.80%yr^{-1} across forests. Changes in controls highlight an even greater shift in burning in forests, with a mean of 2.34-2.42%yr^{-1} for temperate and boreal forests and 2.31-2.58%yr^{-1} for tropical forests. At least 10% of all ecosystems excluding the driest show at least 50% of the maximum possible shift in controls over the study period.

Although some of our results provide evidence of emergent “resource gradient constraints” [16,18,19] (Supplementary Fig. 7), 41% of areas with significant regime shifts would either not be captured by this hypothesis or, by necessity, be attributable to a climate driver, either from positively correlated changes in fuel and moisture controls (Fig. 3e), or independent shifts in fuel alone (Fig. 3f). This demonstrates that controls should be explicitly separated out to attribute fire trends [20].

Our results may be used to inform TBM development and improve their representation of fire, particularly for trends in burnt area. We show that suppression of burnt area by cropland is much greater than the cropland’s own extent, suggesting that landscape fragmentation is an additional mechanism of greater importance than the homogenous cropland representation in most vegetation-fire models [22] (but see [30]). Another important result is that suppression from population density is dramatic [22], drawing attention to the lack of representation of this effect in standard models.

Many recent global fire model developments have focused on the correct representation of fuel and moisture controls [14,22,31,32], arguing that ignitions are less important when reproducing global burnt area [7,8,15]. Our results partially support this hypothesis - areas of ignition limitation tend to occur in areas of even more severe fuel limitation, and have a much smaller “potential” limitation than other controls. However, we also show that many savannas and boreal forest areas are sensitive to small changes in ignitions, where levels of burning are important vegetative controls. The correct representation of ignitions is therefore still crucial for simulating and assessing changing fire regimes under changing climate, land-use and population growth, and projected increases in lightning [33].

It is possible that a more regionalised approach might provide an improved fit to observations of burnt area [34] , but the performance of our global framework (based on globally-invariant parameters) has been shown clearly to be very robust and achieves our objective of simulating the drivers of fire occurrence and frequency, and thereby predicting burnt area statistics within reasonable error. Modelling the impacts of fire on vegetation itself, including mortality and recovery, carbon allocation for resilience and/or recovery and the impact on resultant vegetation distributions is largely unconstrained at coarse global scales [22,32], and would also benefit from studies exploring fire-vegetation impacts [17,18].

We have demonstrated that recent trends in fuel, moisture and suppression controls result in dramatic shifts in burnt area over much of the world. Some of our estimates for trends in fuel and moisture controls could be a consequence of decadal climate variability and may change over a longer period. This study could also be applied to explore how fire regimes might evolve under future climate change [18], particularly when considering temperature targets set by the Paris agreement which, despite being loosely based on perceived widespread ecological and socio-economic thresholds, did not explicitly include changes in fire regime when constructed [36].

Code availability

We were able to find control relationships using a Bayesian Inference framework which could be extended to other areas of high uncertainty in land surface modelling, and which we have made available for use. See https://github.com/rhyswhitley/fire_limitation/ for more information.

Data availability

The data that support the findings in this study are available from the corresponding author upon request.

Correspondence and requests for materials should be addressed to Douglas Kelley (doukel@ceh.ac.uk)

Acknowledgements

The contribution by DK was supported by the UK Natural Environment Research Council through The UK Earth System Modelling Project (UKESM, Grant No. NE/N017951/1). ND was funded by the European Research Council through Reading University (GC2.0 Grant No. 694481). CB's contribution was supported by the Newton Fund through the Met Office Climate Science for Service Partnership Brazil (CSSP Brazil).

Author Contributions

DK and IB devised the modelling framework; RW designed the Bayesian inference framework; DK, IB and CB identified drivers for use within the framework; DK, IB, CB and TM designed the limitation and sensitivity assessments and fire regime shift index.DK, CB and ND collated and regridded input data. DK performed trend analysis. DK wrote the first draft of the paper with input from IB, CB and RW. All authors contributed to the final manuscript. The authors declare no competing interests.

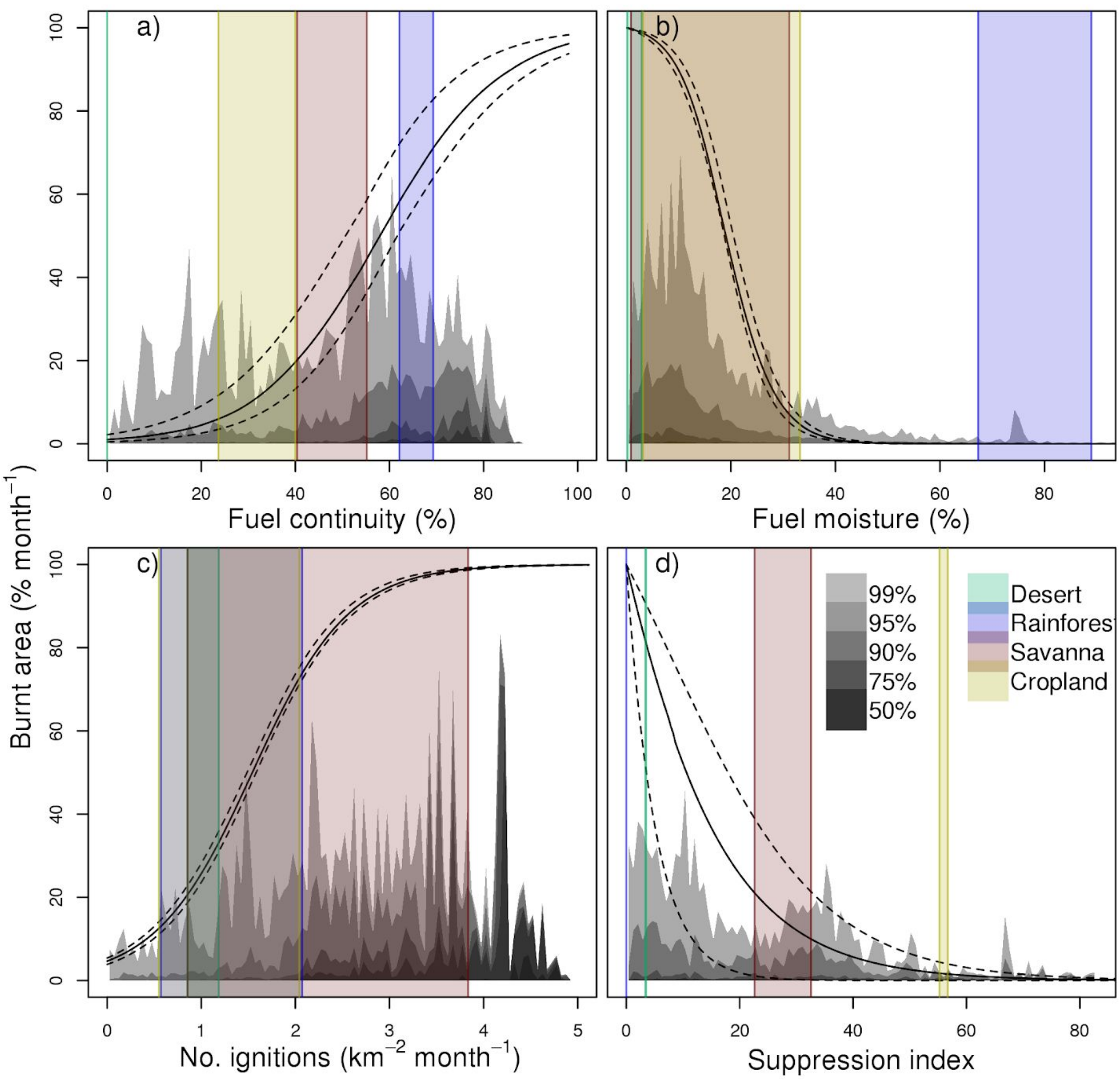

Figure 1: Limitation on burnt area by each control. a) fuel continuity (%); b) fuel moisture (%); c) potential ignitions (km^2 month^{-1}); d) anthropogenic suppression. Black lines show optimized maximum burnt area from each control - solid showing the median and dotted lines the interquartile range of ensemble parameter members. Colours are examples of ranges of controls over the study period for (green) desert (blue) tropical rainforest (red) savanna and (yellow) cropland areas, with locations in Fig. 2. Grey areas indicate quantiles of the observation with 50% of the observations fall under the darkest grey and 99% under the lightest.

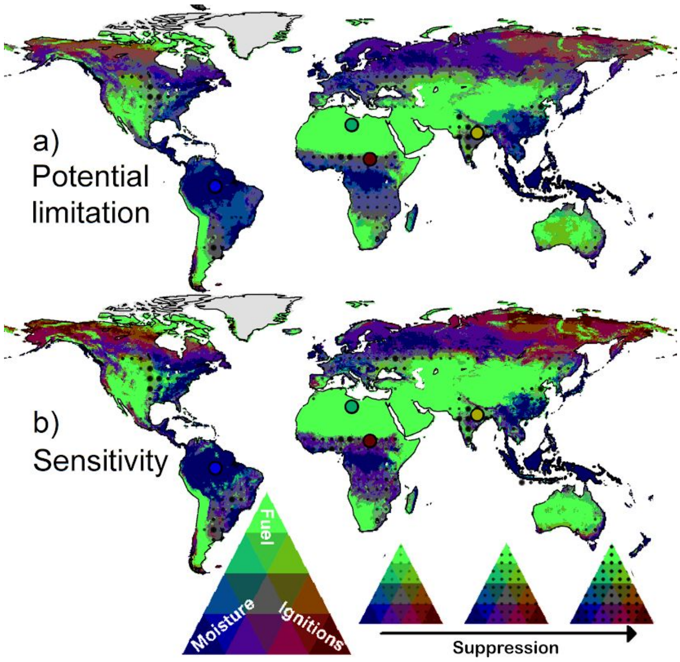

Figure 2: The relative limits and sensitivity imposed on burnt area by each control. Areas are limited by (green) fuel; (blue) moisture; (red) ignitions; (stippled) suppression; (cyan) fuel and moisture; (brown) fuel and ignitions; (magenta) moisture and ignitions; (grey) fuel, moisture and ignitions. Potential limitation shows the increases in burnt area if a control is liberated; sensitivity is the change in burnt area from marginal changes in a control. Coloured dots show the location (green) “desert”; (blue)“rainforest”; (red) “savanna”; (yellow) “cropland” in Fig. 1.

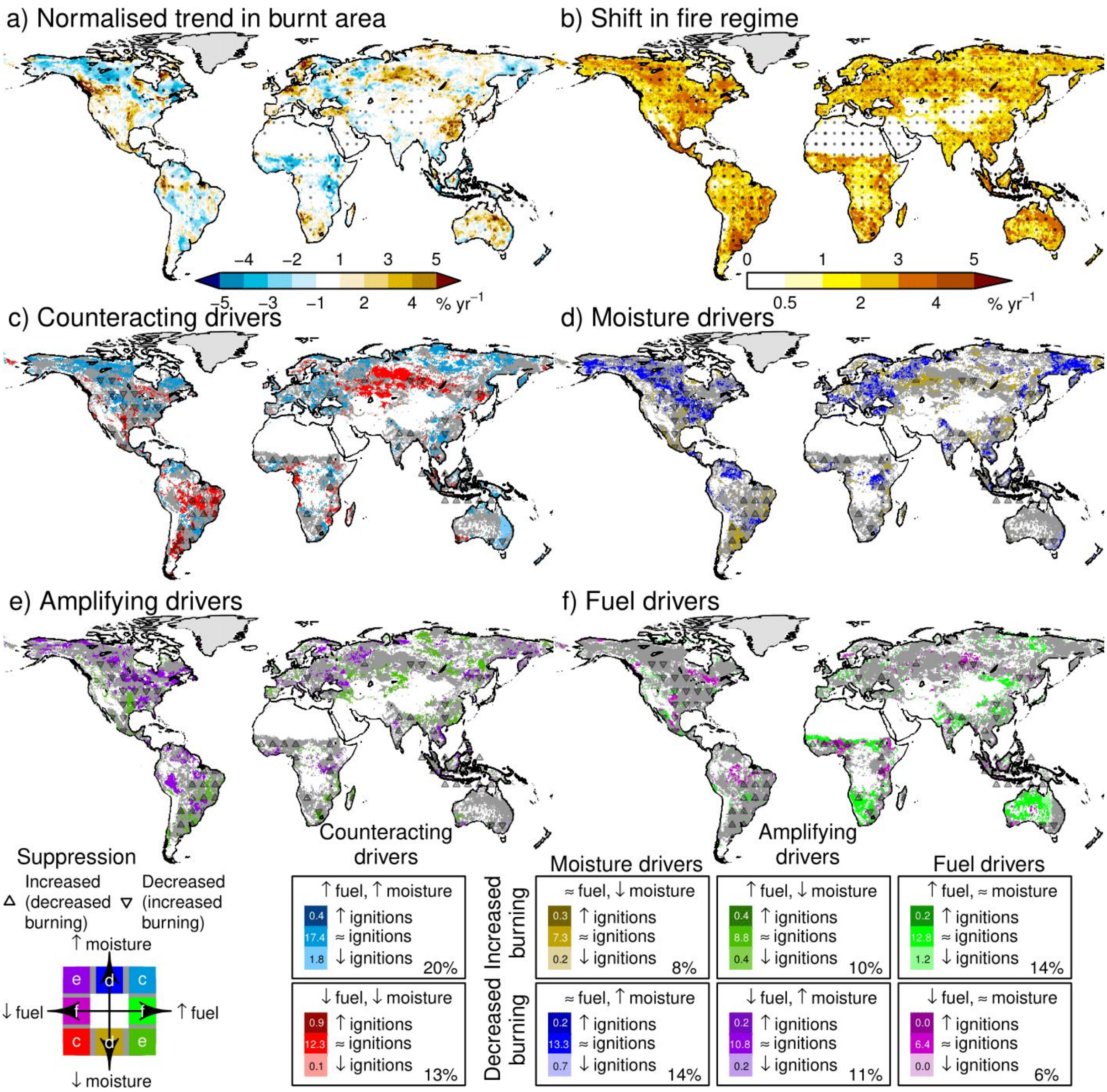

Figure 3: Drivers of trends in burnt area. a) Annual trend in burnt area as a percentage of mean burnt area for the period 2000-2014. b) Absolute change in controls as a percentage of the maximum possible change. Stippled areas in a) and b) are where the sampled posterior parameter standard deviation falls within (light) 50% and (heavy) 10% of the mean change. c-f) Areas with a shift in fire regime equivalent to >50% in at least one control are coloured either grey or c) (cyan) increased fuel and moisture; (red) decreased fuel and moisture; d) (yellow) decrease in fuel moisture, (blue) increases in moisture; e) (lime green) increased continuity and decreased moisture, (violet) decreased fuel and increased moisture; (f) (green) increased fuel continuity, (purple) decrease in fuel. Ignitions increase/decrease represented by darker/lighter colors and increased/decreased suppression by upward/downward arrows respectively. Percentages in legend indicated land area of significant regime shift covered by each fuel and moisture driver combination, and small numbers the breakdown for increase, no change or decrease in ignitions. Individual controls trends can be found in Supplementary Fig. 10.

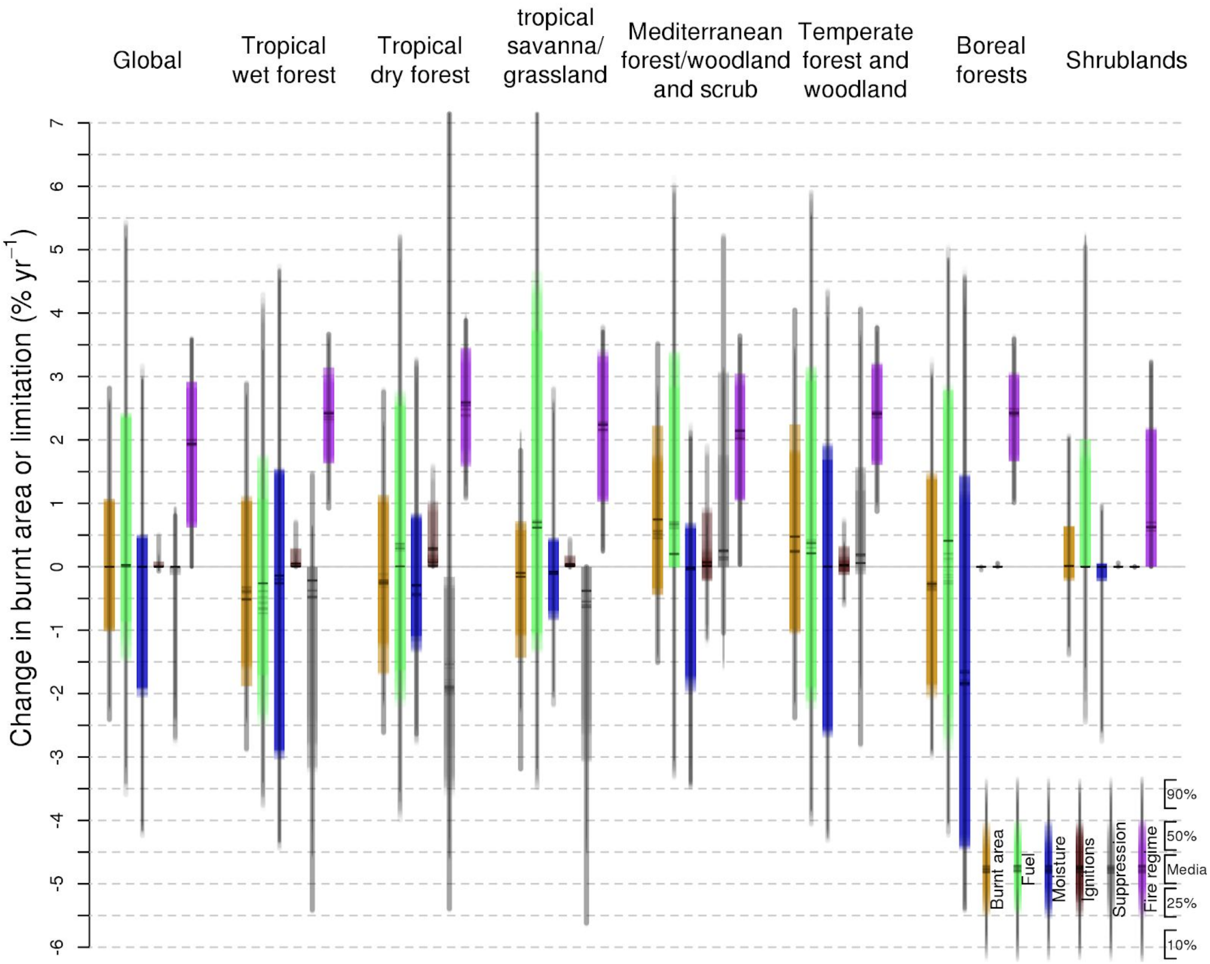

Figure 4: Normalised trends in controls on burnt area from 2000-2014. The first block of 6 boxes shows global trends and subsequent boxes for each vegetation type as defined in Supplementary Fig. 11. Horizontal lines show the median, boxes show the interquartile range and whiskers show a 90% quantile, overlaid for each of 100 randomly selected posterior parameter sets. (orange) the trend in burnt area as a percentage of the fraction of land area for that vegetation type; (green) limitation imposed by fuel controls; (blue) by moisture controls; (brown) anthropogenic ignitions (grey) suppression; (purple) overall shift.

		Global	Tropical wet forest	Tropical dry forest	Tropical savanna/ grass	Med forest/ woodland & scrub	Temp forest & woodland	Boreal forests	Shrub/ Desert
		Burnt area trends							
Burnt area		1.02	1.44	1.24	0.92	1.24	1.48	1.73	0.3
		0.03	0.08	0.13	0.04	0.14	0.11	0.07	0.02
		Control trends							
Fuel		1.81	1.77	2.19	2.42	1.69	2.45	2.56	0.49
		0.15	0.34	0.18	0.13	0.2	0.11	0.1	0.05
Moisture		1.01	2.44	1.07	0.64	1.21	2.19	3.46	0.05
		0.04	0.04	0.09	0.05	0.07	0.08	0.11	0.01
Ignitions		0.02	0.03	0.13	0.04	0.31	0.16	0	0
		0.01	0.02	0.11	0.03	0.18	0.07	0	0
Suppression		0.07	0.93	2.57	0.61	0.97	0.74	0	0
		0.03	0.06	0.2	0.11	0.05	0.15	0	0
		Fire Regime Shift							
Mean		1.92	2.35	2.53	2.14	1.99	2.39	2.38	1.06
		0.02	0.04	0.05	0.03	0.05	0.03	0.04	0.02
Least affected	***10%***	0	0.99	1.18	0.26	0.03	0.93	1.06	0
		0	0.08	0.1	0.03	0.01	0.07	0.03	0
	25%	0.78	1.66	1.69	1.05	1.03	1.63	1.72	0
		0.05	0.05	0.11	0.04	0.03	0.04	0.04	0
	50%	2.01	2.39	2.53	2.2	2.08	2.41	2.45	0.4
		0.03	0.05	0.08	0.05	0.06	0.03	0.04	0.04
	75%	2.95	3.04	3.37	3.29	2.96	3.18	3.03	1.99
		0.05	0.09	0.1	0.07	0.09	0.04	0.04	0.04
Most affected	***90%***	3.61	3.62	3.9	3.71	3.59	3.77	3.57	3.2
		0.02	0.06	0.04	0.03	0.05	0.04	0.07	0.04

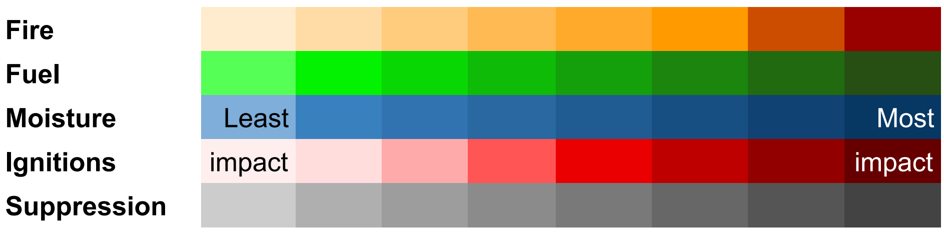

Figure 5: Annual average impacts of trends in controls on burnt area. Row 1, the mean absolute trend in burnt area as a percentage of mean burnt area, rows 2-5 the absolute mean change in burnt area caused by trends in fuel, moisture, ignition and suppression controls. Remaining rows show overall shifts in all controls and the shift for the 10% and 25% most and least affected areas, and median change. Colour indicates the strength of the trend. Supplementary Fig. 11 defines vegetation types. Top numbers in each box show mean whilst bottom shows standard deviation across parameter ensemble members.

References

1. Knorr, W., Arneth, A. & Jiang, L. Demographic controls of future global fire risk. *Nat. Clim. Chang.* **6**, 781–785 (2016).
2. Andela, N. *et al.* A human-driven decline in global burned area. *Science* **356**, 1356–1362 (2017).
3. Giglio, L., Randerson, J. T. & van der Werf, G. R. Analysis of daily, monthly, and annual burned area using the fourth-generation global fire emissions database (GFED4). *Journal of Geophysical Research: Biogeosciences* **118**, 317–328 (2013).
4. Arora, V. K. & Melton, J. R. Reduction in global area burned and wildfire emissions since 1930s enhances carbon uptake by land. *Nat. Commun.* **9**, 1326 (2018).
5. Lasslop, G., Brovkin, V., Reick, C. H., Bathiany, S. & Kloster, S. Multiple stable states of tree cover in a global land surface model due to a fire-vegetation feedback. *Geophys. Res. Lett.* **43**, 6324–6331 (2016).
6. Gelman, A. *et al. Bayesian Data Analysis, Third Edition*. (CRC Press, 2013).
7. Kelley, D. I. Modelling Australian fire regimes. (Macquarie University, 2014).
8. Forkel, M. *et al.* A data-driven approach to identify controls on global fire activity from satellite and climate observations (SOFIA V1). *Geoscientific Model Development* **10**, 4443–4476 (2017).
9. Abatzoglou, J. T., Williams, A. P., Boschetti, L., Zubkova, M. & Kolden, C. A. Global patterns of interannual climate-fire relationships. *Glob. Chang. Biol.* (2018). doi:10.1111/gcb.14405
10. Jolly, W. M. *et al.* Climate-induced variations in global wildfire danger from 1979 to 2013. *Nat. Commun.* **6**, 7537 (2015).
11. Burton, C., Betts, R. A. & Jones, C. D. Will fire danger be reduced by using Solar Radiation Management to limit global warming to 1.5 C compared to 2.0 C? *Geophys. Res. Lett.* (2018).

12. De Groot, W. J., Goldammer, J. G., Justice, C. O. & Lynham, T. J. Implementing a global early warning system for wildland fire. *Proc. Virchow. Pirquet. Med. Soc.* (2010).
13. Kelley, D. I. & Harrison, S. P. Enhanced Australian carbon sink despite increased wildfire during the 21st century. *Environ. Res. Lett.* **9**, 104015 (2014).
14. Prentice, I. C. *et al.* Modeling fire and the terrestrial carbon balance. *Global Biogeochem. Cycles* **25**, (2011).
15. Bistinas, I., Harrison, S. P., Prentice, I. C. & Pereira, J. M. C. Causal relationships versus emergent patterns in the global controls of fire frequency. *Biogeosciences* **11**, 5087–5101 (2014).
16. Van Der Werf, G. R., Randerson, J. T., Giglio, L., Gobron, N. & Dolman, A. J. Climate controls on the variability of fires in the tropics and subtropics. *Global Biogeochem. Cycles* **22**, (2008).
17. Williams, A. P. & Abatzoglou, J. T. Recent Advances and Remaining Uncertainties in Resolving Past and Future Climate Effects on Global Fire Activity. *Current Climate Change Reports* **2**, 1–14 (2016).
18. Krawchuk, M. A. & Moritz, M. A. Burning issues: statistical analyses of global fire data to inform assessments of environmental change. *Environmetrics* **25**, 472–481 (2014).
19. Krawchuk, M. A. & Moritz, M. A. Constraints on global fire activity vary across a resource gradient. *Ecology* **92**, 121–132 (2011).
20. Mann, M. L. *et al.* Incorporating Anthropogenic Influences into Fire Probability Models: Effects of Human Activity and Climate Change on Fire Activity in California. *PLoS One* **11**, e0153589 (2016).
21. Parisien, M.-A. *et al.* The spatially varying influence of humans on fire probability in North America. *Environ. Res. Lett.* **11**, 075005 (2016).
22. Hantson, S. *et al.* The Status and Challenge of Global Fire Modelling. *Biogeosciences* **13**, 3359–3375 (2016).

23. van der Werf, G. R. *et al.* Global fire emissions estimates during 1997–2016. *Earth System Science Data* **9**, 697–720 (2017).

24. van der Werf, G. R. *et al.* Interannual variability in global biomass burning emissions from 1997 to 2004. *Atmos. Chem. Phys.* **6**, 3423–3441 (2006).

25. Marthews, T. R., Burslem, D. F. R. P., Phillips, R. T. & Mullins, C. E. Modelling Direct Radiation and Canopy Gap Regimes in Tropical Forests. *Biotropica* **40**, 676–685 (2008).

26. Balch, J. K. *et al.* Negative fire feedback in a transitional forest of southeastern Amazonia. *Glob. Chang. Biol.* **14**, 2276–2287 (2008).

27. Lapola, D. M. *et al.* Pervasive transition of the Brazilian land-use system. *Nat. Clim. Chang.* **4**, 27–35 (2014).

28. Kauppi, P. E., Sandström, V. & Lipponen, A. Forest resources of nations in relation to human well-being. *PLoS One* **13**, e0196248 (2018).

29. Ciais, P. *et al.* Carbon and other biogeochemical cycles. in *Climate change 2013: the physical science basis. Contribution of Working Group I to the Fifth Assessment Report of the Intergovernmental Panel on Climate Change* 465–570 (Cambridge University Press, 2014).

30. Rabin, S. S. *et al.* A fire model with distinct crop, pasture, and non-agricultural burning: use of new data and a model-fitting algorithm for FINAL. 1. *Geoscientific Model Development* **11**, 815 (2018).

31. Knorr, W., Kaminski, T., Arneth, A. & Weber, U. Impact of human population density on fire frequency at the global scale. *Biogeosciences* **11**, 1085–1102 (2014).

32. Kelley, D. I., Harrison, S. P. & Prentice, I. C. Improved simulation of fire–vegetation interactions in the Land surface Processes and eXchanges dynamic global vegetation model (LPX-Mv1). *Geoscientific Model Development* **7**, 2411–2433 (2014).

33. Romps, D. M., Seeley, J. T., Vollaro, D. & Molinari, J. Climate change. Projected increase in lightning strikes in the United States due to global warming. *Science* **346**,

851–854 (2014).

34. Lehmann, C. E. R., Archibald, S. A., Hoffmann, W. A. & Bond, W. J. Deciphering the distribution of the savanna biome. *New Phytol.* **191**, 197–209 (2011).

Methods

Modelling framework

Monthly burnt area (F) was calculated as a product of limitations imposed by four controls: fuel (dis)continuity (w) represented by vegetation cover, scaled by maximum 12-monthly plant available moisture anomaly ($\frac{\alpha_{max}}{\alpha_{mean}}$ - where α is the ratio of actual to potential evapotranspiration); fuel moisture (ϖ) represented by α, fractional tree cover and atmospheric drying potential; ignition availability (ig) represented by lightning strikes, population density and pasture cover; and direct human suppression (s) represented by cropland and population density (Supplementary Fig. 2). Each control was expressed as a linear combination of its respective drivers and represented by a simple logistic curve (Fig. 1):

$$f(x) = 1 / (1 + e^{-k(x - x_o)})$$

$$F = F_{max} \cdot \Pi f(x) \tag{1}$$

Where $f(x)$ is the limitation imposed by control x (where x takes one of w, ϖ, ig, s), and F_{max} is a maximum permitted monthly burnt area used to aid our model optimization. x_o is the value of control x when it imposes a limitation of 50% on burnt area (i.e, $f(x) = 0.5$), and k is the steepness of the logistic curve, equal to ¼ of the gradient at $x = x_o$. We used the logistic function to describe controls on burnt area because logits are restricted to the [0,1] domain, and this conveniently allows for a product of terms that proportionally modify the key variable of burnt area. $k > 0$ for liberative controls w and ig, where burnt area increases with the control, and $k < 0$ for suppressive ϖ and s, for which burnt area decreases.

As fuel control is liberative and moisture is suppressive, and as the effects of these controls tend to be anticorrelated, our framework replicates the unimodal relationship with burnt area (Supplementary Fig. 7) previously identified along moisture or production gradients [14,19,24,37–39]. With the exception of w, each control was represented by a combination of drivers (x_i) weighted by their respective influences (v_i). Where possible, units are consistent across drivers within each control, and so the combined drivers were normalised to maintain these units:

$$x = \Sigma_i v_i x_i / \Sigma_i v_i \text{ and } v_1 = 1 \tag{2}$$

w was represented by total fractional vegetation cover (C)[40]. C is only provided on an annual timestep, and there are some months in savanna and shrubland areas with very large burnt areas at very low annual average vegetation fractions (Supplementary Fig. 1a). This coincides with areas which experience very short periods of increased available moisture (Supplementary Fig. 1b), probably due to rapid accumulation of fine, flammable fuel loads during a year of seasonal water availability, where a given vegetation fraction is likely to contribute more to fuel continuity than the same, evergreen fraction in non-seasonal areas [41–43]. In order to capture the impact of seasonal variations of moisture on semi-arid ecosystem vegetation cover, we weighted C by the maximum α anomaly over the previous 12 months including the current month (α_{max}), normalised by the annual mean from the previous 12 months (α_{mean}). This follows similar seasonal, water availability metrics used as a proxy for fuel load in other studies [16,20,44]. α was calculated from CRUTS3.23 cloud cover, temperature and precipitation [45] using the STASH model [46] (Supplementary Fig. 2). Fractional cover was also raised to a power (p) in order to account for saturation for high coverage:

$$w = C^p \cdot (v \cdot \left(\frac{\alpha_{max}}{\alpha_{mean}} - 1\right) + 1)/(1 + v) \tag{3}$$

Where v is an optimized weighting parameter. Both C and $\frac{\alpha_{max}}{\alpha_{mean}} - 1$ can be expressed as percentages, and as with equation 2, the denominator means that the fuel controls is also a percentage.

ϖ is a combination of live fuel, dead fuel drying potential, and the impact of the canopy on atmospheric moisture content. Live fuel moisture was represented by α. Dead fuel drying potential follows [32] using CRU relative humidity, temperature, wet days and precipitation [45]. MODIS Vegetation Continuous Fields (VCF) fractional tree cover [40] was used as a proxy of canopy effects on moisture. As α, fuel drying potential and tree cover are all expressed as percentages, combining them using equation (2) means that our moisture control is also a percentage.

ig combines natural ignitions from climatological LIS/OTD lightning flash counts[47], with inter-cloud flashes removed using the technique described by [32], and human-caused ignitions represented by HYDEv3.1 pasture cover and population density [35].

s combines HYDE population density and cropland [35]. As population density contributes to both liberative and suppressive controls, we were able to test and reproduce the humped relationship between fire and population [1,21,31,48] by explicitly representing both of its effects on ignitions and fire suppression (Supplementary Fig. 7). Splitting population between ignitions and suppression allows a more causal representation of population on fire than in previous studies [15,20]. However, population density and our land use drivers still represent more complex mechanisms that could cause a decrease, for example, in burned area when population is increasing as a result of multiple drivers (e.g. a more fragmented and managed landscape, active suppression efforts or an increase due to human accidental/deliberate ignitions or control burns).

All variables were resampled to the coarsest (and most common) resolution of 0.5° using the r raster package [49], with the exception of VCF, where tiles were merged and resampled to 0.5° using gdal [50]. Fractional cover and HYDE variables were interpolated from an annual to a monthly timestep. LIS lightning 12-month climatology was recycled each year. Equations 1 to 3 constitutes our predictive burnt area model, with 17 unknown parameters that were optimised using a form of heuristic search technique. Parameters are global, and therefore the contribution of each driver to a control depends solely on the value of that driver in a given location and time. However, drivers can still affect burnt area in different locations depending on the relative strengths of each control.

Bayesian optimization

The model framework was optimized against the GFED version 4 [3] with small fires [51] dataset (GFED4s) [23] for the period July 2000 to June 2014 (the common years among all datasets) using Bayesian inference. Bayes's theorem states that the likelihood of the values β of the unexplained parameter set (i.e. all $-k,\ x_0$ and F_{max} in equation 1, v_i in equation 2 and $p,\ V$ in equation 3), given a set of observations X, is proportional to the prior probability distribution of β ($P(\beta)$) by the probability of X give β. i.e.

$$P(\beta|X) \propto P(\beta) \cdot P(X|\beta) \tag{4}$$

No prior knowledge of the parameter values were assumed, and bounded uniform priors were used for all parameters, i.e. bounds that were only physically plausible, but generously large [6]. For the sake of simplicity, the model error was defined as normally distributed:

$$P(\beta|X) = \aleph(F,\ \sigma) = \frac{N}{\sigma\sqrt{2\pi}} exp\left\{\Sigma_i^N\left(\frac{y_i - F_i}{\sigma_i}\right)^2\right\} \tag{5}$$

where i represents an individual data point, y_i is the GFED4s burnt area observation, σ is the standard error, and *N* is the observation sample size. Given that the sample size is relatively large, the likelihood information dominated over the priors, such that the optimization reduced to a maximum likelihood problem. Consequently, inferring the posterior solution was a case of minimising equation 5. The posterior solutions were inferred for the models' parameters using a Metropolis-Hastings Markov Chain Monte Carlo (MCMC) step, running 5 chains with 10,000 iterations using [52,53] each over 10% randomly sampled data points on a 0.5°, monthly time step for 14 years; this represented a sample size of 2,314,512 data points. The logistic representation on controls (equation 1) is particularly well suited to inference using Monte-Carlo sampling, as it avoids pathologies in the posterior space that become computationally unreasonable. Unless otherwise stated, the analysis was conducted on a posterior solution constructed by sampling 100 parameter ensemble members from the last 5000 iterations of each chain. Final parameter values and distributions are shown in Supplementary Fig. 4.

Standard, potential and sensitivity to limitation

Using the same logistic function for all controls allowed comparison of the strength of different measures on impact and trends across all controls. “Standard” limitation refers to the limitation imposed by each control under otherwise ideal burning conditions and was defined as $1 - f(x)$ (point along the curve in Fig. 1). “Potential” limitation (p_i) for control i was defined as the potential increase in burnt area if the limitation imposed by a control is removed, in the presence of other controls:

$$p_i = F_{max} \cdot \Pi_j^{N(\hat{i})} f(x_j) = F / f(x_i) \tag{6}$$

(i.e. the product of all fire controls excluding the one being considered). In Supplementary Table 3 and in the text, the potential increase from the removal of a control is simply the difference in potential limitation and reconstructed burnt area ($p_i - F$).

The sensitivity to limitation (S_i) was defined as the change in burnt area (G) relative to the maximum rate of change in burnt area for that control (i.e when $x = x_0$), weighted by the potential limitation for that cell:

$$G = \frac{\delta f(x)/\delta x}{\delta f(x_0)/\delta x}$$

$$S_i = G_i \cdot p_i \tag{7}$$

Framework assessment

The Bayesian inference model contains a framework error parameter which describes the standard deviation of reconstructed fire from GFED4s observations. This was normalised by

GFED4s observed deviation to help interpret the deviation between observations and each parameter combination. This is similar to the Normalised Mean Squared Error benchmarking method described in [54], but for each month rather than an annual average. As recommended by Fire Model Intercomparison Project (FireMIP) [55], we also used the non-square metrics from [54] to assess each parameter combination's ability to reconstruct the annual average burnt area and spatial trends in burnt area. The difference between reconstructed annual average burnt area from a given parameter set (sim) and observed (obs) was assessed using the Normalised Mean Error (NME) metric, which sums the difference over all cells (i) weighted by cell area (A_i) and normalises by the average distance from the mean of observations ($\overline{obs}$):

$$NME = \frac{\sum A_i \cdot |sim_i - obs_i|}{\sum A_i \cdot |obs_i - \overline{obs}|} \tag{8}$$

NME comparisons were conducted in three steps:

1. As described above;
2. With obs_i and sim_i taking the difference between observations or simulation and their respective means. ie $x_{i,\,step\,2} = x_i - \bar{x}$ removing systematic bias and describing the performance of the model around the mean.
3. obs_i and sim_i from step 2 were divided by the mean deviation. i.e $x_{i,\,step3} = x_{i,\,step\,2}/|x_{i,\,step2}| = (x_i - \bar{x})/|x_i - \bar{x}|$ This transformation removes the influence of the variability and describes the models' ability to reproduce the spatial pattern in burnt area.

The trend in burnt area was assessed on a 12-month running mean to remove seasonal effects. As burnt area assumes values in the standard unit interval [0, 1], a logit transformation was performed on both simulated and observed burnt area to assess trends relative to the annual average burnt area, taking into account maximum or minimum possible burnt area bounds. This removes model error in spatial patterns already assessed by equation 8 from our assessments of trends. Furthermore, as burnt area can take extremes of 0 and 1, an initial transformation was required so that bounds become (0, 1):

$$x \rightarrow (x \cdot (n-1) + 0.5)/n$$

$$x \rightarrow ln\left(\frac{x}{1-x}\right) \tag{9}$$

Where, in this case, x is burnt area and n is the number of timesteps, in this case, 168 months.

The burnt area trend was calculated for each grid cell using a simple linear regression model

$$x = x_0 + \frac{\delta x}{\delta t}t \tag{10}$$

The difference in $\frac{\delta x}{\delta t}$ between observations and simulation were compared using NME in order to assess spatial variations in temporal trends (equation 8). Non-significant trends in the observations (i.e, p-value > 0.1) were not compared.

The smaller the NME score, the closer the simulation to observation, with a perfect score (i.e., simulation that perfectly matches observations) of 0. Three null models were used to help interpret the score. The mean null model is the score obtained by comparing the mean of all observations with the observations. As NME is normalised by the mean difference, NME s mean null model score is always 1. The best "single value" model was obtained by comparing the median of observations to observations, and its score is by definition less than or equal to the mean model score for NME. The randomly resampled null model compares randomly-resampled observations (without replacement) to the observations. As this score obtained was different depending on resampling order, 1000 bootstraps were used to describe three randomly resampled null models: the mean randomly resampled score and ± the standard deviation of our bootstrap. Randomly resampled bootstraps were almost always worse than the median and mean null models.

Our reconstructed annual average burnt area obtained an NME score of 0.60-0.63 vs GFED4s and 0.73-0.78 against other FireMIP benchmark datasets (Supplementary Table 2), which outperformed all null models, and is better than published assessments of other global vegetation-fire models using the same comparison method [22,37,48,54,56], although most of these are driven by simulated vegetation and fuel. Similar scores for step 1 to 3 NME suggests our spatial pattern in burnt areas also performs well. Our spatial variations in trends in burnt area (Supplementary Fig. 6) scores of 0.75-0.88 were also better than null models, beating the median null model by approximately the same percentage as our annual average scores.

As well as performing well in spatial patterns and trends in burnt area, our optimized control strength (Fig. 1,2) and trends (Fig. 3) matches with field studies and greenhouse experiments. Moisture limits burnt area to 10% at moistures of 29% (±0.15%), similar to studies of fuel moisture content levels that prohibit fire [57–59]. Fuel allows 50% monthly burning at 55%±0.01% fuel continuity which equates to roughly 87% of total vegetative cover (equation 3), meaning some limitation is still experienced in forested ecosystems. This is backed up by repeat burn studies which suggest forests can become fuel limited after removal of ground fuel [26,39]. The Eastern USA is shown to be highly limited by, and sensitive to, human suppression (Fig. 2 and Supplementary Fig. 8), in agreement with [21,60]. We also reproduced the transition from ignition/climate sensitive burnt area in northern and coastal California to fuel sensitive fire regions in southern inland California that has been found other studies [20]. And we reproduce the climate-induced drying trend that is causing an increase in fire in Western USA [61] (Fig. 3c,d, Supplementary Fig. 10)

Trend analysis

Trends were calculated for burnt area by fitting a simple linear regression model as described in equation 9 & 10 for each month of the year over our time period. We also calculated trends for each control in the same way to assess its impact on burnt area. Because lightning ignition data was provided as a climatology, we only show the impact of population density on ignition trends. Trends were removed from each control, leaving behind just seasonal and interannual variability. The impact of the trend in control i ($\frac{\delta F_t}{dx_i}$) is the reconstructed burnt area with the control's trend removed:

$$\frac{\delta F_t}{dx_{i\ t}} = f_i(x_{i,t} - t \cdot \frac{\delta x_i}{dt}) \cdot p_{i,\,t}$$

(11)

The difference between this and reconstructed burnt area including the trend (i.e F in equation 1) was summed over our study period, and normalised between -100% and 100% to describe the maximum possible decrease or increase in burnt area due to trends in the control:

$$D(x_i) = \int_0^t F_t - \frac{\delta F_t}{dx_{i\ t}}\, dt \;/\overline{F}$$

$$\overline{F} = max(\int_0^t F_t\, dt\,,\ \int_0^t \frac{\delta F_t}{dx_{i\ t}}\, dt) \tag{12}$$

As this measure is normalised to total burnt area over the study period, the time units cancel and the measure is the change in fractional burnt area over the period. Dividing by the number of years in the study period (14 years) expresses $D(x_i)$ as the change in burnt areas per year in Fig. 3,5. This also forms the basis of a measure of the overall shift in fire regime over the study period ($D_{|All|}$). The overall change in our controls was quantified as the Euclidean distance between the potential impact of controls with and without detrending. This was normalised by the maximum possible change in potential limitation (i.e. when the change in a given control over our study period is ±1) which is $\sqrt{no.\ controls} = 2$. As there are 4 controls, the change in fire regime is therefore determined by:

$$D_{|All|} = \sqrt{\Sigma_i(\,D(x_i))^2}/2 \tag{13}$$

$D_{|All|}$ is equal to 0 if there is no change in controls, 1 if all controls change by the maximum possible, and 0.5 if one control changes by its maximum and with equal potential amongst all controls. This is similar to the square chord distance used in fire model evaluations to measure the difference between four items in two different datasets [54,55], with the potential limitation of each control taking the place of an “item”.

A shift in fire regime was described as robust and significant (Fig 3c) if >95% of ensemble members show a $D_{|All|}$ of > 0.25 over the study period - equivalent to a 50% shift in burnt area from one control if all other controls stay constant. A given control shows a robust contribution to this shift if >95% of ensemble members agree on the direction of the control’s trend (equation 12). The control with the largest trend is defined as significant, and additional controls are also significant if the 90% of ensemble members show a contribution of greater than 10% of the control with the largest trend.

References

35. Klein Goldewijk, K., Goldewijk, K. K., Beusen, A., Van Drecht, G. & De Vos, M. The HYDE 3.1 spatially explicit database of human-induced global land-use change over the past 12,000 years. *Glob. Ecol. Biogeogr.* **20**, 73–86 (2010).
36. Knutti, R., Rogelj, J., Sedláček, J. & Fischer, E. M. A scientific critique of the two-degree climate change target. *Nat. Geosci.* **9**, 13–18 (2015).
37. Kloster, S. & Lasslop, G. Historical and future fire occurrence (1850 to 2100) simulated in CMIP5 Earth System Models. *Glob. Planet. Change* **150**, 58–69 (2017).
38. Moritz, M. A. *et al.* Climate change and disruptions to global fire activity. *Ecosphere* **3**, 1–22 (2012).
39. Bradstock, R. A. A biogeographic model of fire regimes in Australia: current and future implications. *Glob. Ecol. Biogeogr.* (2010).
40. Dimiceli, C. *et al.* MOD44B MODIS/Terra Vegetation Continuous Fields Yearly L3 Global 250m SIN Grid V006. (2015). doi:10.5067/MODIS/MOD44B.006
41. Barone, J. A. Effects of light availability and rainfall on leaf production in a moist tropical

forest in central Panama. *J. Trop. Ecol.* **14**, 309–321 (1998).

42. Valim, E. A. R., Nalini, H. A., Jr & Kozovits, A. R. Litterfall dynamics in a iron-rich rock outcrop complex in the southeastern portion of the Iron Quadrangle of Brazil. *Acta Bot. Brasilica* **27**, 286–293 (2013).
43. Leigh, E. G., Jr. *Tropical Forest Ecology: A View from Barro Colorado Island*. (Oxford University Press, 1999).
44. Krawchuk, M. A., Moritz, M. A., Parisien, M.-A., Van Dorn, J. & Hayhoe, K. Global pyrogeography: the current and future distribution of wildfire. *PLoS One* **4**, e5102 (2009).
45. Harris, I., Jones, P. D., Osborn, T. J. & Lister, D. H. Updated high-resolution grids of monthly climatic observations - the CRU TS3.10 Dataset. *Int. J. Climatol.* **34**, 623–642 (2013).
46. Davis, T. W. *et al.* Simple process-led algorithms for simulating habitats (SPLASH v.1.0): robust indices of radiation, evapotranspiration and plant-available moisture. *Geoscientific Model Development* **10**, 689–708 (2017).
47. Cecil, D. J., Buechler, D. E. & Blakeslee, R. J. Gridded lightning climatology from TRMM-LIS and OTD: Dataset description. *Atmos. Res.* **135-136**, 404–414 (2014).
48. Burton, C. *et al.* Representation of fire, land-use change and vegetation dynamics in the Joint UK Land Environment Simulator vn4. 9 (JULES). *Geoscientific Model Development* **12**, 179–193 (2019).
49. Hijmans, R. J. & van Etten, J. raster: Geographic data analysis and modeling. *R package version* **2**, (2014).
50. GDAL/OGR contributors. *GDAL/OGR Geospatial Data Abstraction software Library*. (Open Source Geospatial Foundation, 2018).
51. Randerson, J. T., Chen, Y., van der Werf, G. R., Rogers, B. M. & Morton, D. C. Global burned area and biomass burning emissions from small fires. *Journal of Geophysical*

Research: Biogeosciences **117**, (2012).

52. Salvatier, J., Wiecki, T. V. & Fonnesbeck, C. Probabilistic programming in Python using PyMC3. *PeerJ Comput. Sci.* **2**, e55 (2016).
53. Al-Rfou, R. *et al.* Theano: A Python framework for fast computation of mathematical expressions. *arXiv preprint* (2016).
54. Kelley, D. I. *et al.* A comprehensive benchmarking system for evaluating global vegetation models. *Biogeosciences* **10**, 3313–3340 (2013).
55. Rabin, S. S. *et al.* The Fire Modeling Intercomparison Project (FireMIP), phase 1: Experimental and analytical protocols. *Geoscientific Model Development* **10**, 1175 (2017).
56. Lasslop, G., Thonicke, K. & Kloster, S. SPITFIRE within the MPI Earth system model: Model development and evaluation. *Journal of Advances in Modeling Earth Systems* **6**, 740–755 (2014).
57. Brown, J. K., Intermountain Forest and Range Experiment Station (Ogden & Utah). *Field test of a rate-of-fire-spread model in slash fuels /*. (1972).
58. Blackmarr, W. H. *Moisture Content Influences Ignitability of Slash Pine Litter*. (1972).
59. Danson, F. M. & Bowyer, P. Estimating live fuel moisture content from remotely sensed reflectance. *Remote Sens. Environ.* **92**, 309–321 (2004).
60. Staal, A. *et al.* Resilience of tropical tree cover: The roles of climate, fire, and herbivory. *Glob. Chang. Biol.* (2018). doi:10.1111/gcb.14408
61. Dennison, P. E., Brewer, S. C., Arnold, J. D. & Moritz, M. A. Large wildfire trends in the western United States, 1984--2011. *Geophys. Res. Lett.* **41**, 2928–2933 (2014).

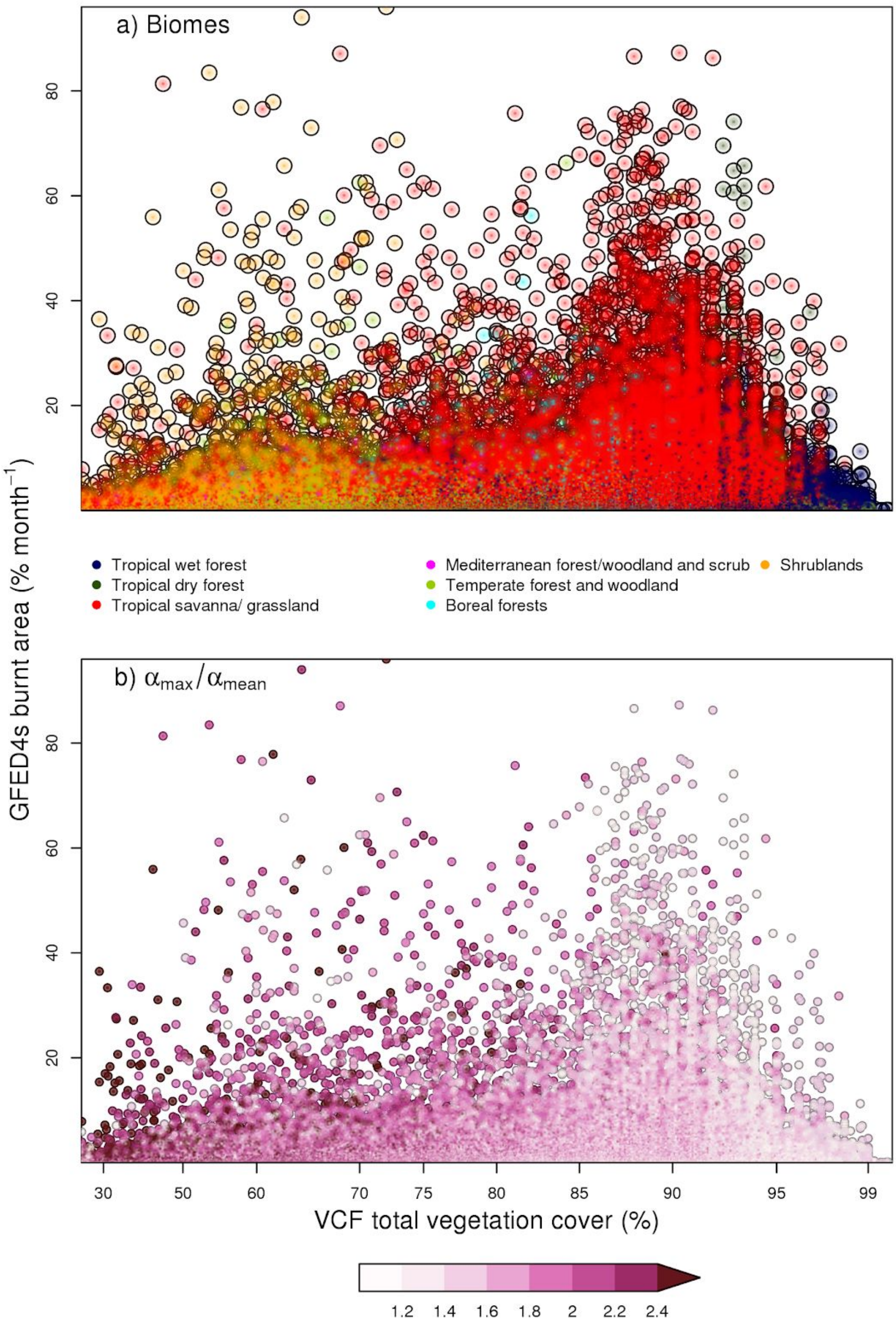

Supplementary Figure 1: **Vegetation fraction vs monthly burnt area.** Vegetation cover taken from VCF [1] is used as a driver for fuel continuity controls, and burnt area from GFED4s [2] is the target dataset used to optimize the framework. Areas with no burning are masked out. a) coloured by vegetation types. The main 4 types that containing fire are, from humid to arid, (blue) tropical wet forest; (green) tropical dry forest; (red) tropical savanna and grass; (orange) shrubland. See Supplementary Fig. 11 for vegetation types definitions. b) coloured by $\frac{\alpha_{max}}{\alpha_{mean}}$, with highly seasonal (high $\frac{\alpha_{max}}{\alpha_{mean}}$) in dark shades and non-seasonal in light. Note the transformation on the x-axis using $x^{3.18}$ - where the power, p is the median of the optimized value in equation 3 when $v = 0$ (i.e no influence of $\frac{\alpha_{max}}{\alpha_{mean}}$).

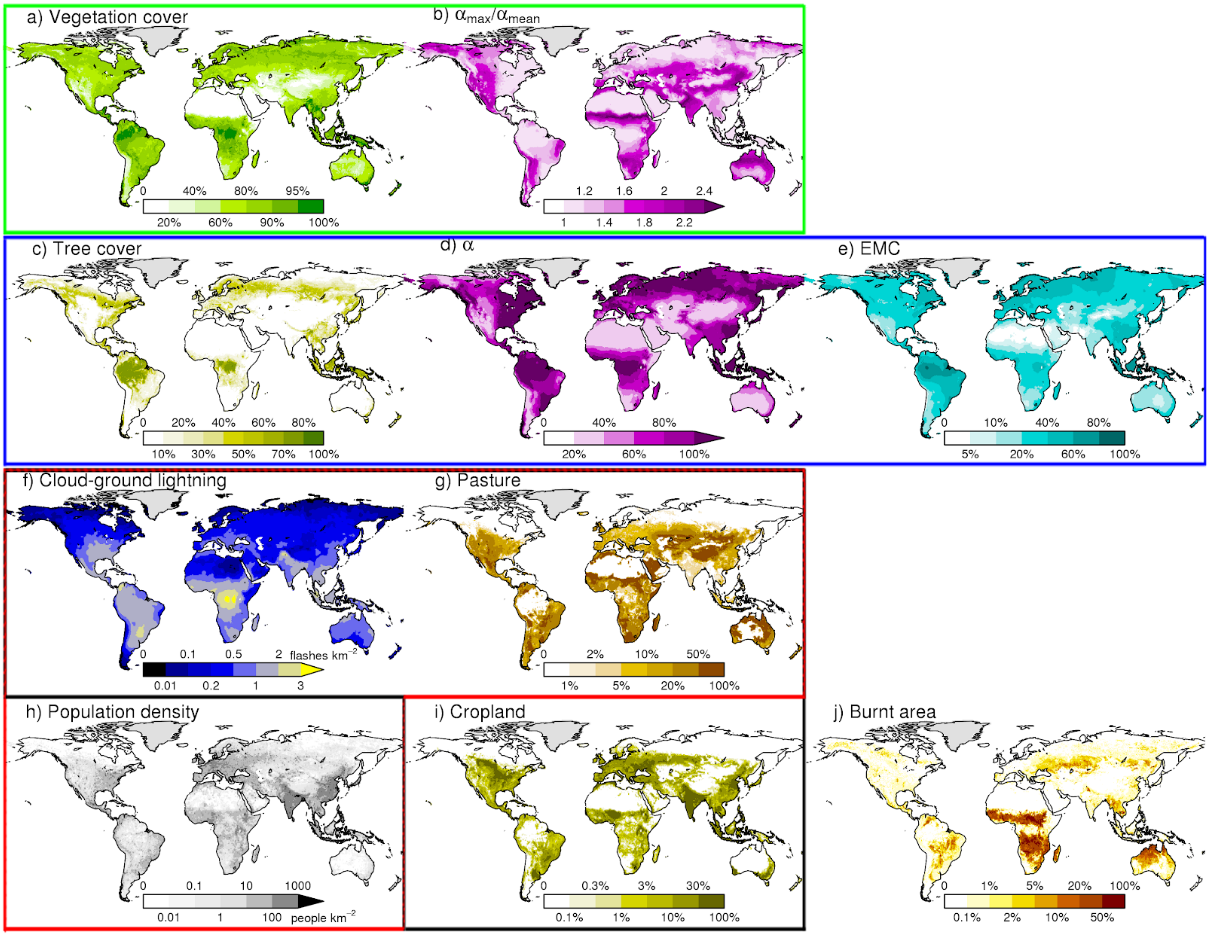

Supplementary Figure 2: Mean annual values for the variables used to reconstruct burnt area. Green box contains variables used to describe fuel continuity control: a) total percentage vegetation cover [3]; b) annual maximum monthly over mean annual actual over potential evapotranspiration anomaly ($\frac{\alpha_{max}}{\alpha_{mean}}$) calculated using the SPLASH model [4]. Blue box contains variables used for fuel moisture: c) percentage tree cover [3]; d) mean annual actual over potential evapotranspiration (α) [4]; e) equilibrium moisture content (EMC) calculated as per [5]. Red box contains variables used for ignitions: f) number of lightning flashes from LIS [6] corrected for cloud-to-ground strikes following [5]; g) percentage pasture cover [7]; f) population density [7]. Black box contains variables used for anthropogenic suppression which, in addition to f), includes g) percentage cropland cover [7]. h) is the mean annual burnt area [2] the framework is optimized against.

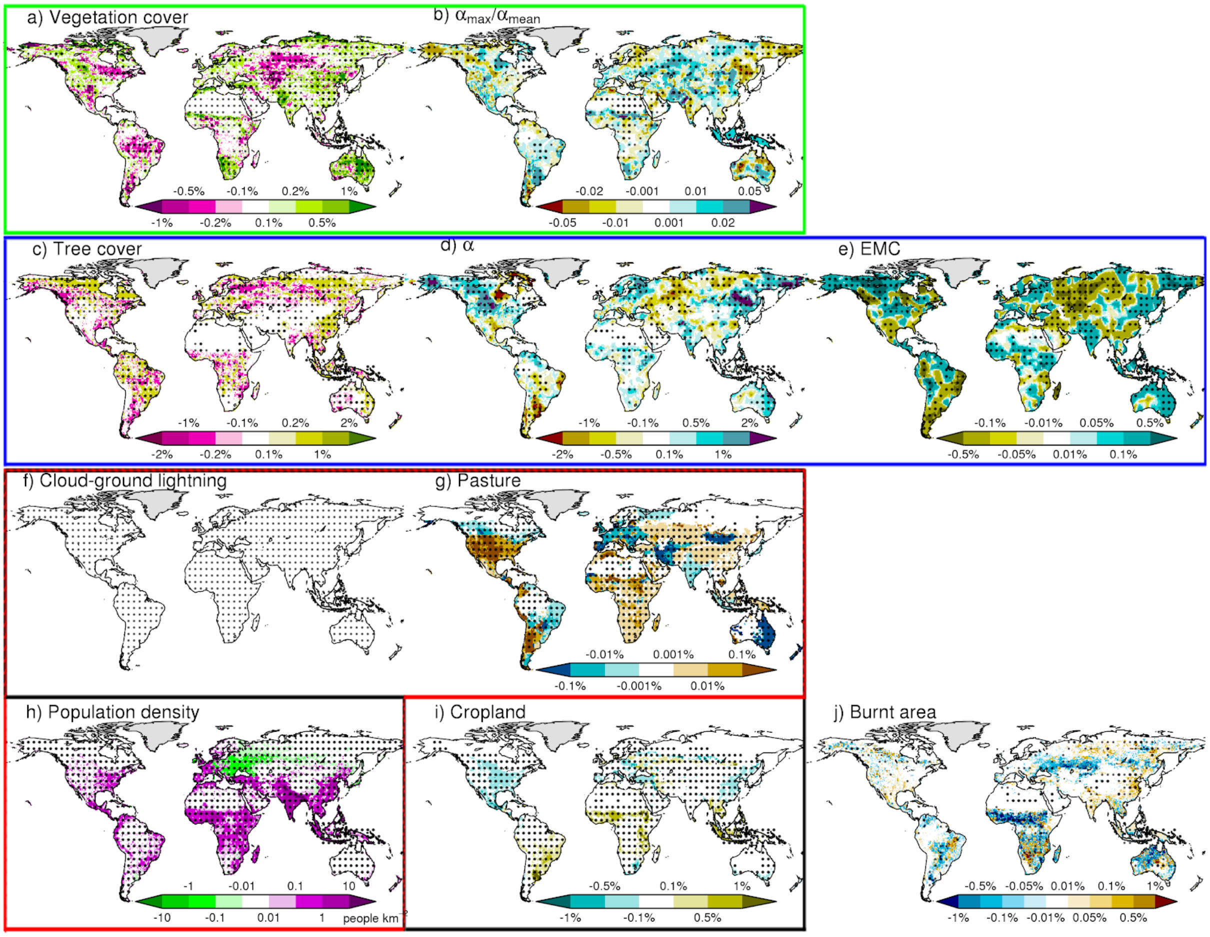

Supplementary Figure 3: **Mean annual trends for the variables used to reconstruct burnt area.** Shows the same drivers and the same units as in Supplementary Fig. 1. Fitted using a simple linear model (equation 11 in methods). Stippling show significance in trends, measured on dx/dt in methods equation 8: light stippling is where $0.01 < p-value < 0.1$, heavy stippling is where $p-value < 0.01$.

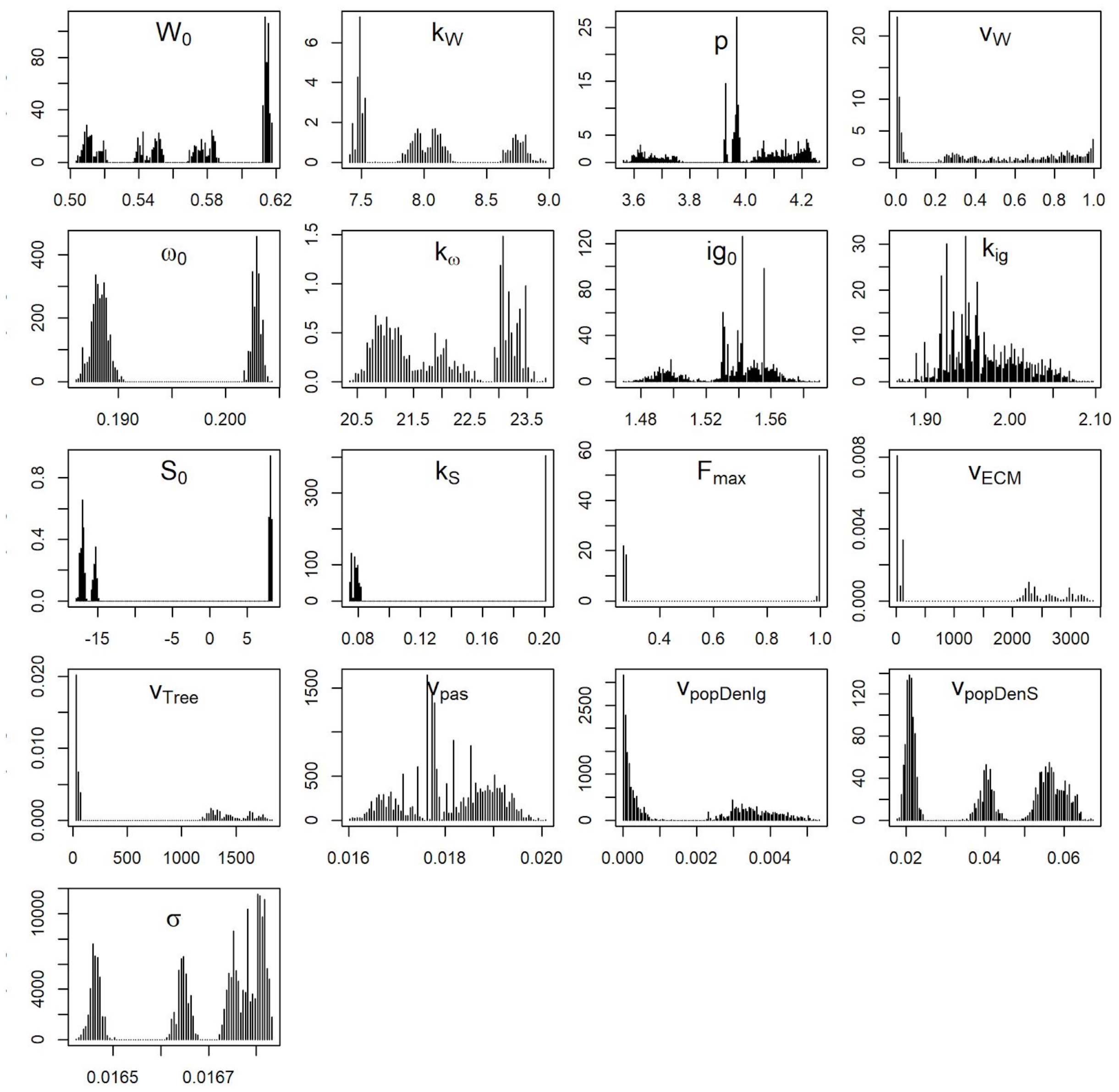

Supplementary Figure 4: Probability distributions used to reconstruct burnt area and its controls. Parameters are described in equations 1-3 in methods, obtained using the Bayesian inference technique outlined in equations 4-5 in methods. See methods for parameter definitions.

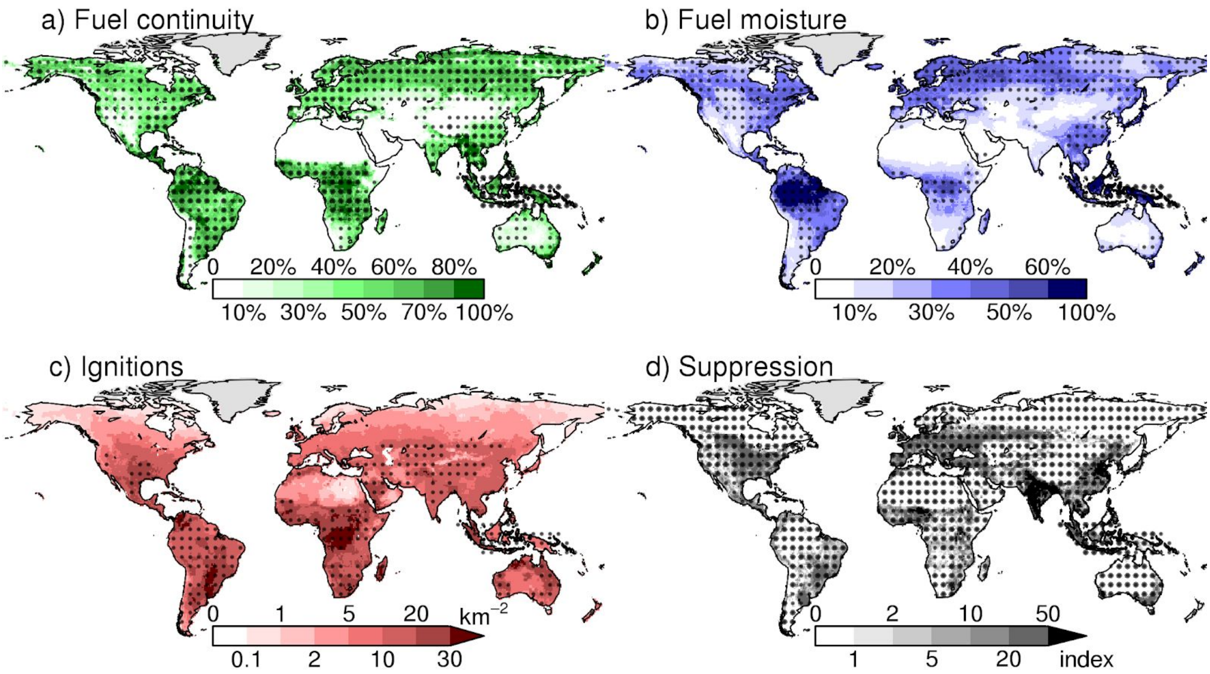

Supplementary Figure 5: Mean monthly controls on burnt area. a) fuel continuity (%); b) fuel Moisture (%); c) ignitions (km^{-2} month^{-1}); d) anthropogenic suppression. Light stippling showing where 90% of ensemble members falling within 10% of the ensemble mean and heavy showing 99% falling within 10% of the ensemble mean.

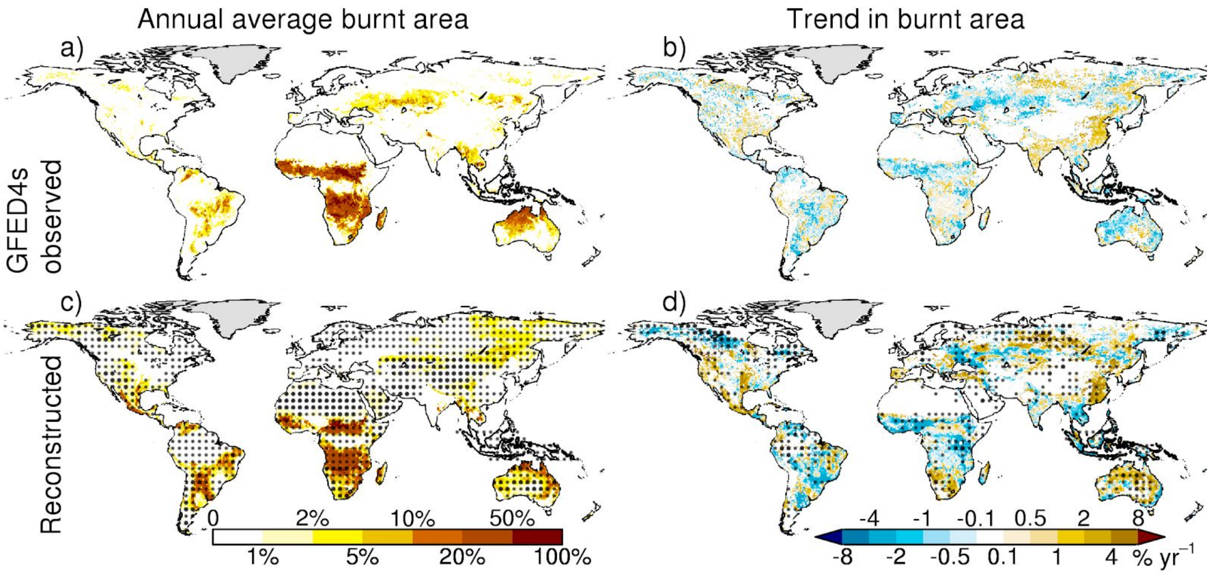

Supplementary Figure 6: Comparison of reconstructed vs. observed burnt area. a, c show annual % burnt area and b, d yearly mean trends in burnt area normalised by burnt area for 2000-2014 for (top row, a, b) GFED4s observations and (bottom, c, d) reconstructed burnt area, with light stippling showing where 90% of ensemble members falling within 10% of the ensemble mean and heavy showing 99% falling within 10% of the ensemble mean.

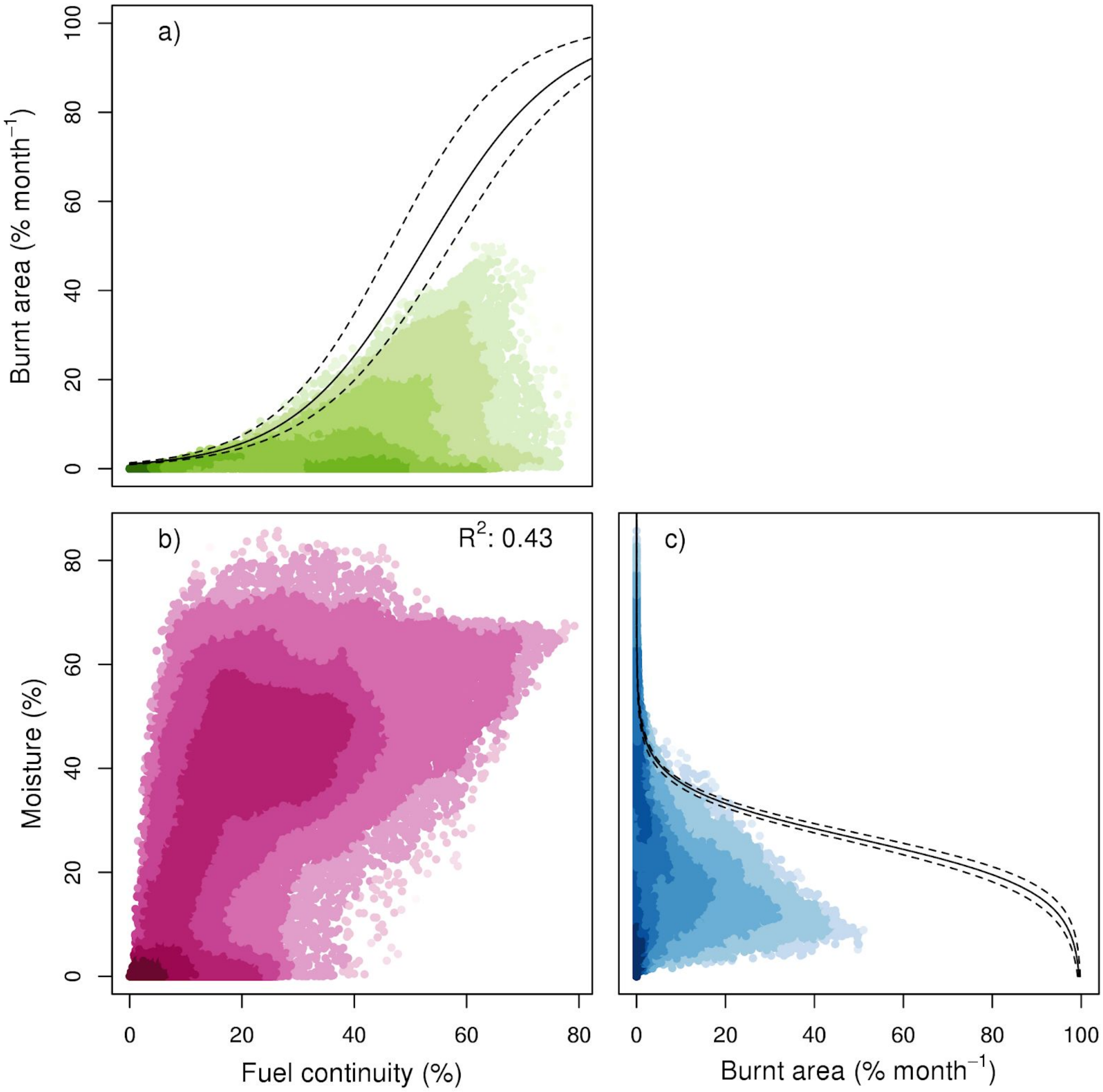

Supplementary Figure 7: Emergent unimodal gradient from fuel and moisture controls. a and c show moisture and fuel controls respectively vs burnt area. Lines show maximum allowed burnt area for the given control (i.e. the same lines as Fig. 1). Solid black lines show optimized maximum possible burnt area for a given value of that control, using the median ensemble parameter values. Dotted lines show the interquartile range of our parameter ensemble members (see Methods). Density cloud shows the mean monthly maximum burnt area from the interaction of fuel and moisture controls (i.e max. from fuel × max. from moisture). b) fuel control vs moisture control, with the R^2 value given in the top right-hand corner.

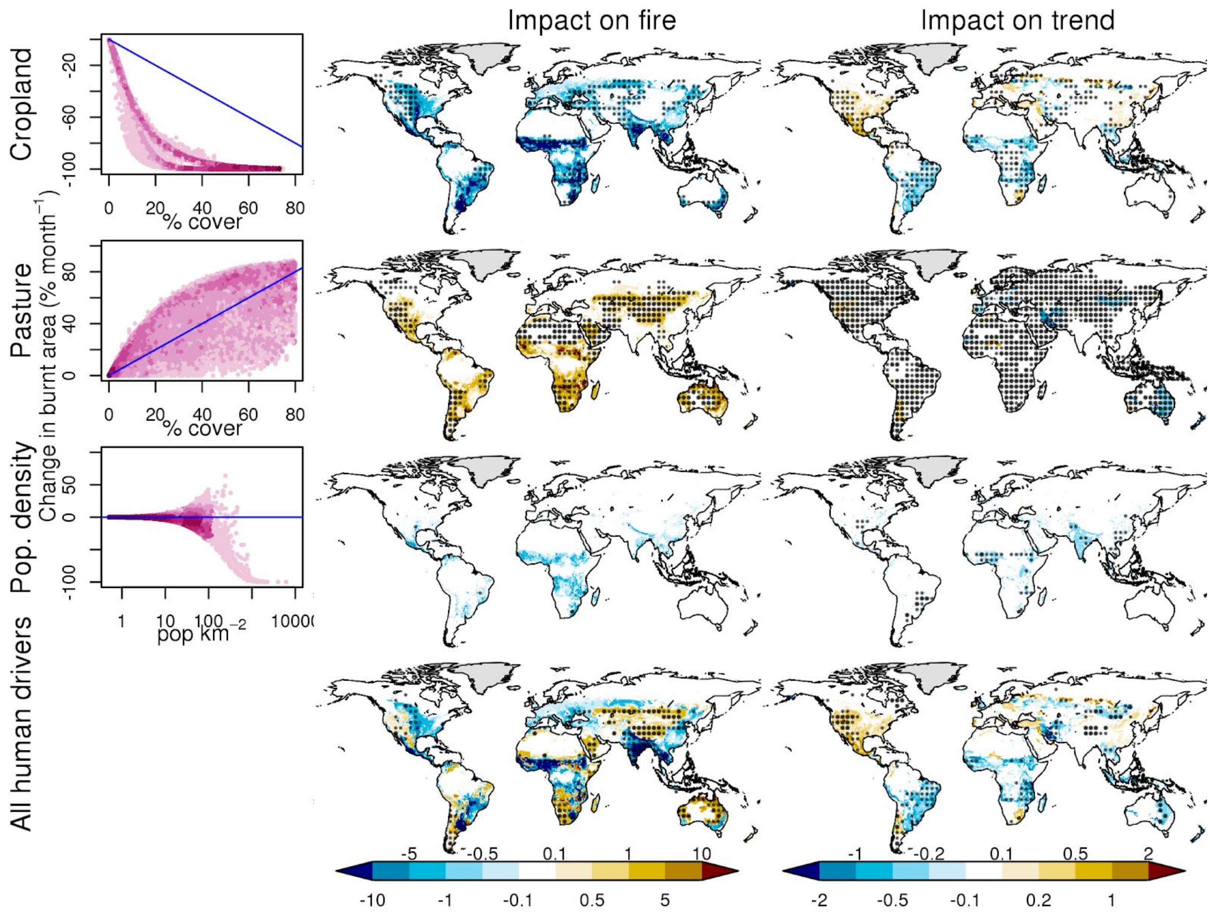

Supplementary Figure 8: **Cropland, pasture and population density impact on burnt area.** In the first column, the impact of each driver (x-axis) on burnt area (y-axis) is calculated as the difference in burnt area reconstructed with and without each variable as a percentage of the burnt areas without that variable. The percent annual average of this difference is mapped in the second column. The percent annual mean impact on burnt area of each driver in the 3rd column is calculated as per equation 11-12 in methods, but with trends in each variable removed instead of an entire control. The 1st row shows the impact of cropland, 2nd shows the impact of pasture, 3rd population density and the 4th row show the impact of all three drivers. Light stippling shows where 90% of ensemble members falling within 10% of the ensemble mean and heavy showing 99% falling within 10% of the ensemble mean.

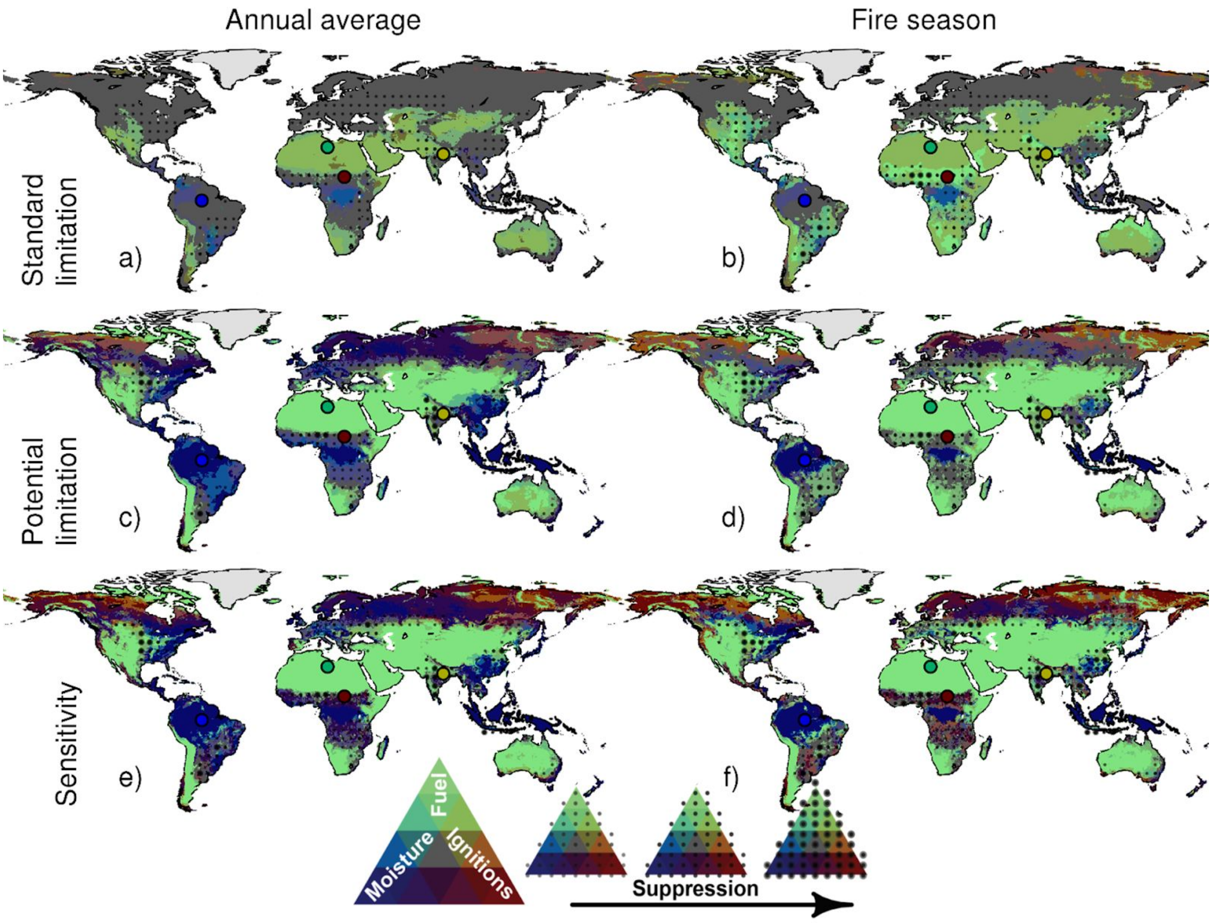

Supplementary Figure 9: **Spatial variation of the relative limits imposed on burnt area by each control.** Green areas are predominantly fuel limited, blue are moisture limited, red by ignitions and stippled by suppression. Combined shades demonstrate co-limitation: (cyan) fuel and moisture; (brown) fuel and ignitions and (magenta) moisture and ignitions. Grey areas are equally limited by all coloured controls. Standard limitation is the limitation by each control in isolation of other controls (i.e., points on the curve in Fig. 1); potential limitation shows relative increases in burnt area if control is fully liberated in the presence of other controls; sensitivity is the change in burnt area from marginal changes in control in the presence of other controls. The 1st column shows the annual average limitations or sensitivity; the 2nd column the average limitation or sensitivity during the climatological month of the maximum reconstructed burnt area in each cell (i.e. month when equation 1 is maximised). Dots show the locations of coloured sections in Fig. 1, with green showing the location of “desert”, blue “rainforest”, red “savanna” and yellow “cropland”.

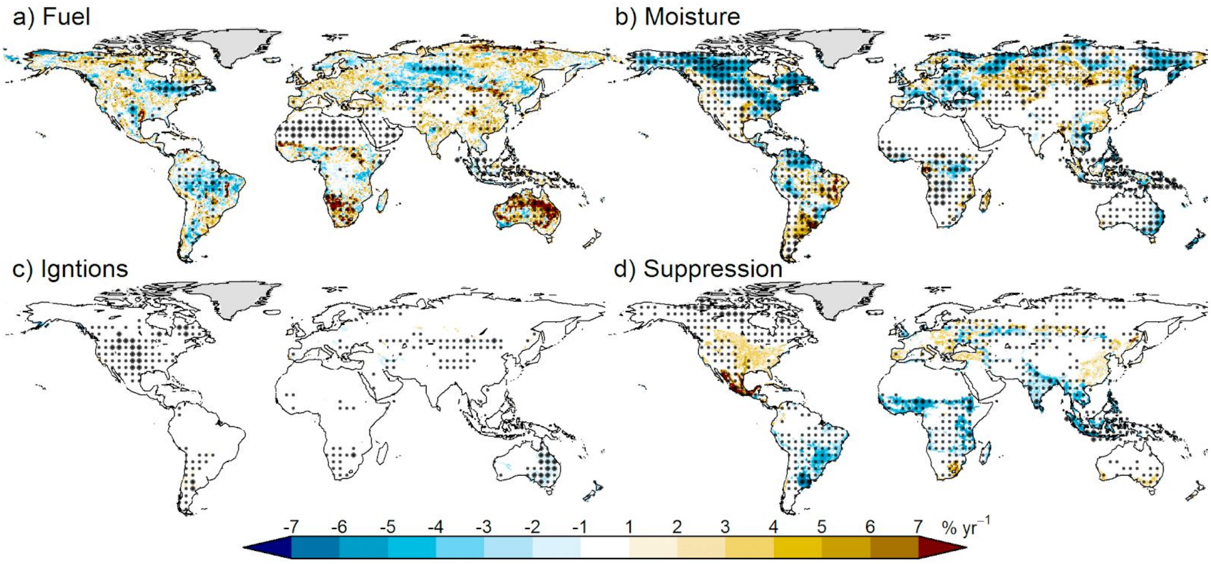

Supplementary Figure 10: The impact on burnt area of each control between 2000-2014 as a percentage of the maximum possible change in burnt area. a) fuel continuity; b) fuel moisture; c) ignitions; d) anthropogenic suppression. See equation 12 in methods. Blue shows reductions in burnt area, yellow and brown increases. Light stippling shows where 90% of ensemble members falling within 10% of the ensemble mean and heavy showing 99% falling within 10% of the ensemble mean.

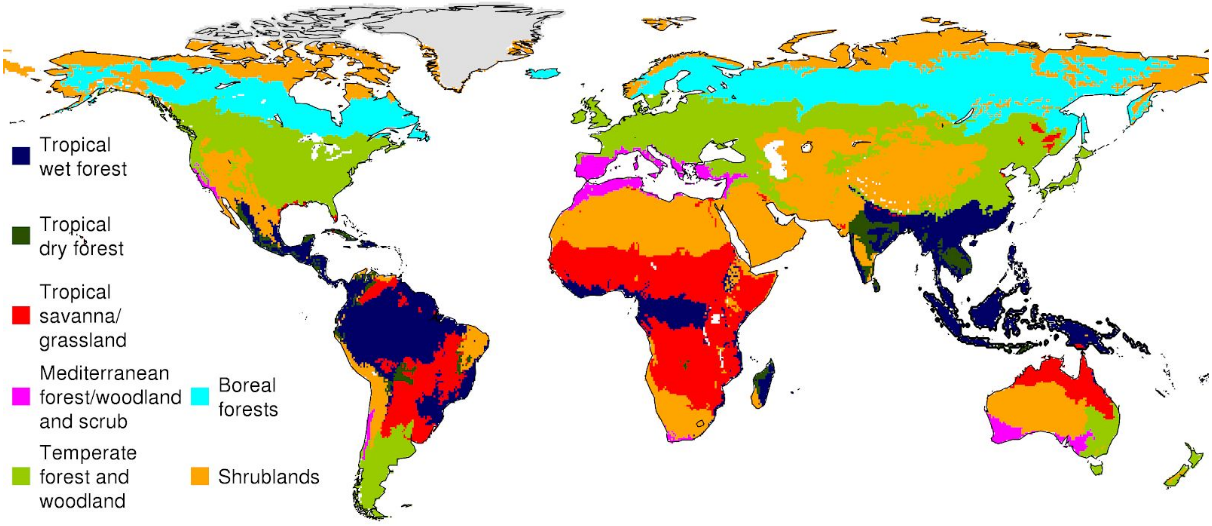

Supplementary Figure 11: **Ecosystems defined by grouping vegetation types from [8].** Tropical wet forests are defined as tropical & subtropical wet broadleaf forest, tropical and subtropical coniferous forests[8]; tropical dry forest as tropical and subtropical broadleaf dry forest, tropical savanna/grassland as tropical and subtropical grasslands, savannas and shrublands, wooded grasslands & savannas; mediterranean forest/woodland and scrub as mediterranean forests, woodlands and scrub; temperate forest and woodland as temperate broadleaf and mixed forests, temperate grasslands, savannas & shrublands, temperate conifer forests; boreal forests as boreal forests/taiga; shrublands as montane grasslands and shrublands, tundra, deserts and xeric shrublands.

Supplementary Tables

Supplementary Table 1: Controls and their driving variables. "Calculated as" column describes how, or cites from where, the variable was calculated. "Driver represented" described what aspect, or driver, of a given control the variable represents.

Control	Variable	Calculated as	Driver represented	Data source
Fuel continuity "Fuel" (%)	Total vegetation cover (%)	1 - bare cover	Allowed fire spread	MODIS Vegetation Continuous Fields (VCF) [1]
	Maximum seasonal anomalies in water availability	$\frac{\alpha_{max}}{\alpha_{mean}} - 1$ (see row below)	Rapid seasonal accumulation of fire fuel	CRUTS3.23 relative humidity, temperature, wet days & precipitation [9]
Fuel moisture "Moisture" (%)	α (%)	Actual:potential evapotranspiration - SPLASH model [4]	Live fuel moisture proxy	CRUTS3.23 cloud cover, temperature & precipitation [9]
	Equilibrium fuel moisture content (%)	Kelley et al [5]	Dead fuel moisture proxy	CRUTS3.23 relative humidity, temperature, wet days & precipitation [9]
	Tree Cover (%)		Canopy effects on moisture.	VCF [1]
Potential ignitions "Ignitions" (no. km^{-2})	Lightning strikes (strikes km^{-2})	Cloud-to-ground as per Kelley et al [5]	Natural ignitions	LIS/OTD lightning flash counts[6]
	Population density (people km^{-2})		Human ignitions	HYDEv3.1[7]
	Pasture (%)		Pasture fires [10]	
Anthropogenic suppression "Suppression"	Cropland (%)		Land use fragmentation	
	Population density (people/km^2)		Fragmentation/ landscape management and fuel reductions	

Supplementary Table 2: Performance of reconstructed fire against burnt area observations. Uses the metrics described by equation 6-8 in methods. Datasets are the same used in the FireMIP benchmarking protocol [11,12], with references given in the table. Scores are provided for the best (min), worst (max) and by score quantiles across our sampled posterior. Colouring follows [12] where, in this case, blue scores are better than all null models, and green is better than all but one.

Comparison	Metric	Step	Null Models				Reconstructed fire score quantiles						
			Median	*Mean*	*Randomly Resampled*								
					Mean	*Sd*	*Min*	*10%*	*25%*	*50%*	*75%*	*90%*	**Max**
Model error	NMSE	1	1.00	1.00	1.743	0.005	0.772	0.800	0.804	0.818	0.826	0.833	0.853
GFED4s [2] annual average 2000-2014	NME	1	0.745	1.00	1.167	0.002	0.603	0.612	0.613	0.623	0.627	0.629	0.63
		2					0.598	0.606	0.61	0.625	0.629	0.632	0.637
		3					0.615	0.62	0.623	0.625	0.655	0.665	0.677
MERIS [13] annual average 2006-2009		1	0.691	1.00	1.120	0.003	0.699	0.713	0.720	0.733	0.750	0.752	0.755
		2					0.704	0.720	0.724	0.753	0.785	0.787	0.792
		3					0.642	0.647	0.648	0.650	0.679	0.693	0.705
MCD45 [14] annual average 2001-2009		1	0.722	1.00	1.150	0.003	0.708	0.712	0.718	0.757	0.797	0.799	0.803
		2					0.718	0.721	0.725	0.784	0.841	0.843	0.848
		3					0.653	0.659	0.666	0.673	0.674	0.685	0.694
GFED4s [2] trends 2000-2014		1	0.957	1.00	1.044	0.004	0.85	0.852	0.852	0.873	0.876	0.878	0.881
		2					0.877	0.877	0.878	0.894	0.897	0.9	0.901
		3					0.923	0.924	0.925	0.952	0.957	0.959	0.961

Supplementary Table 3: Limitation and sensitivity of controls across different vegetation types. Green rows indicate the strength of fuel controls, blue rows indicate moisture, red ignitions and grey suppression. Standard limitation is the strength of each control in isolation of other controls (i.e, points on the curve in Fig. 1); potential limitation shows relative increases in burnt area if control is fully liberated in the presence of other controls; sensitivity is the change in burnt area from marginal changes in control in the presence of over other controls. Top numbers in each box show mean across our posterior, whilst the bottom shows standard deviation across parameter ensemble members. The most important control for standard or potential limitation for a given vegetation type is in **bold**, the 2nd most important in *italics*.

	Global	***Tropical wet forest***	***Tropical dry forest***	***Tropical savanna /grass***	***Med forest/ wood & Scrub***	***Temp forest & wood***	***Boreal forests***	***Shrub/ Desert***
	Standard							
Fuel	**78.64** **2.84**	*66.76* *1.60*	**80.31** **0.45**	**75.98** **0.86**	**83.91** **0.39**	**83.10** **0.87**	75.41 1.03	**91.47** **0.55**
Moisture	57.62 0.44	**82.13** **0.07**	69.36 0.06	*58.08* *0.13*	67.23 0.07	69.27 0.18	*79.47* *0.08*	37.98 0.25
Ignitions	*67.35* *2.15*	60.10 0.77	*72.14* *0.44*	56.10 0.80	*75.74* *0.42*	*72.74* *0.90*	**84.83** **0.35**	*76.24* *0.87*
Suppression	29.98 1.08	36.56 0.44	36.93 0.25	31.50 0.46	36.48 0.26	45.70 0.59	18.07 0.24	16.94 0.37
	Potential							
Fuel	**20.49** **0.08**	*5.25* *0.01*	**9.32** **0.01**	**30.18** **0.04**	**10.51** **0.01**	**11.39** **0.02**	5.08 0.01	**32.48** **0.04**
Moisture	*9.82* *0.07*	**23.5** **0.06**	*6.01* *0.01*	*12.21* *0.02*	*4.13* *0.01*	*4.01* *0.01*	**5.59** **0.01**	1.93 0.01
Ignitions	3.48 0.03	1.50 0.00	1.97 0.00	3.91 0.01	2.12 0.00	1.9 0.01	*5.85* *0.01*	*2.93* *0.01*
Suppression	4.51 0.05	4.95 0.02	5.44 0.01	8.60 0.02	2.50 0.01	3.64 0.02	1.21 0.00	1.57 0.01
	Sensitivity							
Fuel	2.20 0.02	1.02 0.01	0.38 0.00	0.66 0.01	0.35 0.00	0.89 0.01	0.80 0.01	0.52 0.01
Moisture	0.53 0.01	0.09 0.00	0.07 0.00	0.16 0.00	0.08 0.00	0.16 0.00	0.08 0.00	0.34 0.00
Ignitions	1.33 0.01	0.44 0.00	0.25 0.00	0.40 0.00	0.28 0.00	0.57 0.01	0.27 0.00	0.66 0.01
Suppression	3.34 0.03	1.23 0.01	0.68 0.01	1.27 0.01	0.69 0.01	1.34 0.01	0.96 0.01	1.57 0.02

Supplementary references

1. Dimiceli, C. *et al.* MOD44B MODIS/Terra Vegetation Continuous Fields Yearly L3 Global 250m SIN Grid V006. (2015). doi:10.5067/MODIS/MOD44B.006
2. van der Werf, G. R. *et al.* Global fire emissions estimates during 1997–2016. *Earth Syst. Sci. Data* **9**, 697–720 (2017).
3. Daac, N. L. P. Vegetation Continuous Fields : MOD44B. (2015). doi:10.5067/MODIS/MOD44B.006
4. Davis, T. W. *et al.* Simple process-led algorithms for simulating habitats (SPLASH v.1.0): robust indices of radiation, evapotranspiration and plant-available moisture. *Geoscientific Model Development* **10**, 689–708 (2017).
5. Kelley, D. I., Harrison, S. P. & Prentice, I. C. Improved simulation of fire–vegetation interactions in the Land surface Processes and eXchanges dynamic global vegetation model (LPX-Mv1). *Geoscientific Model Development* **7**, 2411–2433 (2014).
6. Cecil, D. J., Buechler, D. E. & Blakeslee, R. J. Gridded lightning climatology from TRMM-LIS and OTD: Dataset description. *Atmos. Res.* **135-136**, 404–414 (2014).
7. Klein Goldewijk, K., Goldewijk, K. K., Beusen, A., Van Drecht, G. & De Vos, M. The HYDE 3.1 spatially explicit database of human-induced global land-use change over the past 12,000 years. *Glob. Ecol. Biogeogr.* **20**, 73–86 (2010).
8. Olson, D. M. *et al.* Terrestrial Ecoregions of the World: A New Map of Life on Earth A new global map of terrestrial ecoregions provides an innovative tool for conserving biodiversity. *Bioscience* **51**, 933–938 (2001).
9. Harris, I., Jones, P. D., Osborn, T. J. & Lister, D. H. Updated high-resolution grids of monthly climatic observations - the CRU TS3.10 Dataset. *Int. J. Climatol.* **34**, 623–642 (2013).
10. Bistinas, I., Harrison, S. P., Prentice, I. C. & Pereira, J. M. C. Causal relationships versus emergent patterns in the global controls of fire frequency. *Biogeosciences* **11**,

5087–5101 (2014).

11. Rabin, S. S. *et al.* The Fire Modeling Intercomparison Project (FireMIP), phase 1: Experimental and analytical protocols. *Geoscientific Model Development* **20**, 1175–1197 (2017).
12. Burton, C. *et al.* Representation of fire, land-use change and vegetation dynamics in the Joint UK Land Environment Simulator vn4. 9 (JULES). *Geoscientific Model Development* **12**, 179–193 (2019).
13. Alonso-Canas, I. & Chuvieco, E. Global burned area mapping from ENVISAT-MERIS and MODIS active fire data. *Remote Sens. Environ.* **163**, 140–152 (2015).
14. Roy, D. P., Boschetti, L., Justice, C. O. & Ju, J. The collection 5 MODIS burned area product—Global evaluation by comparison with the MODIS active fire product. *Remote Sens. Environ.* **112**, 3690–3707 (2008).